31 Ong HT, Hasegawa K, Dietz AB, Russell SJ, Peng KW. Evaluation of T cells as carriers for systemic measles virotherapy in the presence of antiviral antibodies. *Gene Ther* 2007; **14**: 324–333.
32 Peng KW, Dogan A, Vrana J, Liu C, Ong HT, Kumar S *et al.* Tumor-associated macrophages infiltrate plasmacytomas and can serve as cell carriers for oncolytic measles virotherapy of disseminated myeloma. *Am J Hematol* 2009; **84**: 401–407.
33 Garcia-Castro J, Martinez-Palacio J, Lillo R, Garcia-Sanchez F, Alemany R, Madero L *et al.* Tumor cells as cellular vehicles to deliver gene therapies to metastatic tumors. *Cancer Gene Ther* 2005; **12**: 341–349.
34 Power AT, Bell JC. Cell-based delivery of oncolytic viruses: a new strategic alliance for a biological strike against cancer. *Mol Ther* 2007; **15**: 660–665.
35 Raykov Z, Balboni G, Aprahamian M, Rommelaere J. Carrier cell-mediated delivery of oncolytic parvoviruses for targeting metastases. *Int J Cancer* 2004; **109**: 742–749.
36 Jevremovic D, Gulati R, Hennig I, Diaz RM, Cole C, Kleppe L *et al.* Use of blood outgrowth endothelial cells as virus-producing vectors for gene delivery to tumors. *Am J Physiol Heart Circ Physiol* 2004; **287**: H494–H500.
37 Cole C, Qiao J, Kottke T, Diaz RM, Ahmed A, Sanchez-Perez L *et al.* Tumor-targeted, systemic delivery of therapeutic viral vectors using hitchhiking on antigen-specific T cells. *Nat Med* 2005; **11**: 1073–1081.
38 Confino E, Harlow L, Gleicher N. Peritoneal fluid and serum autoantibody levels in patients with endometriosis. *Fertil Steril* 1990; **53**: 242–245.
39 Stallwood Y, Fisher KD, Gallimore PH, Mautner V. Neutralisation of adenovirus infectivity by ascitic fluid from ovarian cancer patients. *Gene Ther* 2000; **7**: 637–643.
40 Mader EK, Maeyama Y, Lin Y, Butler GW, Russell HM, Galanis E *et al.* Mesenchymal stem cell carriers protect oncolytic measles viruses from antibody neutralization in an orthotopic ovarian cancer therapy model. *Clin Cancer Res* 2009; **15**: 7246–7255.

Trichoplein controls microtubule anchoring at the centrosome by binding to Odf2 and ninein

Miho Ibi[1,*], Peng Zou[1,*], Akihito Inoko[1,*], Takashi Shiromizu[1], Makoto Matsuyama[1,2], Yuko Hayashi[1], Masato Enomoto[1,3], Daisuke Mori[4], Shinji Hirotsune[4], Tohru Kiyono[5], Sachiko Tsukita[6], Hidemasa Goto[1,3] and Masaki Inagaki[1,3,‡]

[1]Division of Biochemistry, Aichi Cancer Center Research Institute, Chikusa-ku, Nagoya 464-8681, Japan
[2]The Foundation for Promotion of Cancer Research, Chuo-ku, Tokyo 104-0045, Japan
[3]Department of Cellular Oncology, Graduate School of Medicine, Nagoya University, Showa-ku, Nagoya 466-8550, Japan
[4]Department of Genetic Disease Research, Osaka City University Graduate School of Medicine, Osaka 545-8586, Japan
[5]Virology Division, National Cancer Center Research Institute, Chuo-ku, Tokyo 104-0045, Japan
[6]Laboratory of Biological Science, Graduate School of Frontier Biosciences/Graduate School of Medicine, Osaka University, Suita, Osaka 565-0871, Japan
*These authors contributed equally to this work
‡Author for correspondence (minagaki@aichi-cc.jp)

Accepted 27 October 2010
Journal of Cell Science 124, 857-864

doi:10.1242/jcs.075705

Summary

The keratin cytoskeleton performs several functions in epithelial cells and provides regulated interaction sites for scaffold proteins, including trichoplein. Previously, we found that trichoplein was localized on keratin intermediate filaments and desmosomes in well-differentiated, non-dividing epithelia. Here, we report that trichoplein is widely expressed and has a major function in the correct localization of the centrosomal protein ninein in epithelial and non-epithelial cells. Immunocytochemical analysis also revealed that this protein is concentrated at the subdistal to medial zone of both mother and daughter centrioles. Trichoplein binds the centrosomal proteins Odf2 and ninein, which are localized at the distal to subdistal ends of the mother centriole. Trichoplein depletion abolished the recruitment of ninein, but not Odf2, specifically at the subdistal end. However, Odf2 depletion inhibited the recruitment of trichoplein to a mother centriole, whereas ninein depletion did not. In addition, the depletion of each molecule impaired MT anchoring at the centrosome. These results suggest that trichoplein has a crucial role in MT-anchoring activity at the centrosome in proliferating cells, probably through its complex formation with Odf2 and ninein.

Key words: Trichoplein, Microtubule (MT), Centriole, Odf2, Ninein, Cell proliferation

Introduction

Intermediate filaments (IFs), together with microtubules (MTs) and actin filaments, form the cytoskeletal framework in the cytoplasm of various eukaryotic cells. Unlike MTs and actin filaments, the protein components of IFs vary in a cell-, tissue- and differentiation-dependent manner. Type I and type II keratin proteins form heterodimers in epithelial cells, and their composition also depends on tissue type and the stage of differentiation. Two heterodimers associate with one tetramer, which assembles into higher-order oligomers and forms 10 nm filaments. Keratin IFs associate with plasma membrane specializations such as desmosomes and hemidesmosomes in the periphery. Similarly to other cytoskeletal IFs, keratin IFs also extend into the cytoplasm where they provide a scaffold for other cytoskeletal elements including centrosome and MTs (Eriksson et al., 1992; Steinert, 1993; Fuchs and Weber, 1994; Fuchs and Cleveland, 1998; Magin et al., 2007; Pekny and Lane, 2007; Godsel et al., 2008; Eriksson et al., 2009).

The centrosome is the primary MT-organizing center in animal cells. It is composed of two orthogonal centrioles surrounded by pericentriolar material from which MTs emanate and elongate. These paired centrioles are structurally distinct, reflecting their different ages. The older one (a mother centriole) functions as a template in the preceding cell cycle and carries distal to subdistal appendages, whereas the younger one (a daughter centriole), which is duplicated in the preceding cell cycle, lacks this structure. The mother centriole directly docks MTs at its appendages, whereas the daughter centriole does not (Bornens, 2002; Bettencourt-Dias and Glover, 2007; Bornens, 2008; Nigg and Raff, 2009).

The dynamics of IF network is well correlated with that of other cytoskeletal networks including centrosome and MTs. IF-associated proteins (IFAPs) are emerging as important regulators that coordinate the remodeling and function of such cytoskeletal networks. Members of the plakin family (such as plectin) were identified as crosslinkers between IFs and other cytoskeletal elements including actin filaments and MTs. Although several IFAPs have been identified as regulators of IF remodeling and function, the function of IFAPs in other cytoskeletal systems is largely unknown (Fuchs and Cleveland, 1998; Houseweart and Cleveland, 1998; Izawa and Inagaki, 2006; Godsel et al., 2008).

Nishizawa and colleagues (Nishizawa et al., 2005) previously reported that trichoplein keratin filament-binding protein (trichoplein or TCHP) serves as a keratin IF scaffold protein. Similarly to another keratin IF scaffold protein, Albatross (Sugimoto et al., 2008), this protein has a trichohyalin and plectin homology domain (TPHD; also see supplementary material Fig. S3A), which has similarities to classical keratin IF scaffold proteins (Izawa and Inagaki, 2006). In villous epithelial (non-dividing) cells of the small intestine, trichoplein mainly colocalizes with keratin IFs and the desmosome (Nishizawa et

al., 2005). Here, we report that trichoplein is concentrated at the subdistal to medial zone of both mother and daughter centrioles in dividing epithelial and non-epithelial cells. RNA interference (RNAi)-mediated trichoplein depletion inhibited MT anchoring at the centrosome. This MT-anchoring activity was regulated by the interaction of trichoplein with two other centriole proteins, Odf2 and ninein.

Results and Discussion

We first produced a rabbit polyclonal antibody against full-length (FL) mouse trichoplein. In total cell lysates of EpH4, MTD1A (mouse mammary epithelial) or NIH3T3 (mouse fibroblastic), anti-mouse trichoplein reacted specifically with a band corresponding to mouse trichoplein, which shared 77% homology with human trichoplein (Fig. 1A). Treatment with mouse trichoplein-specific

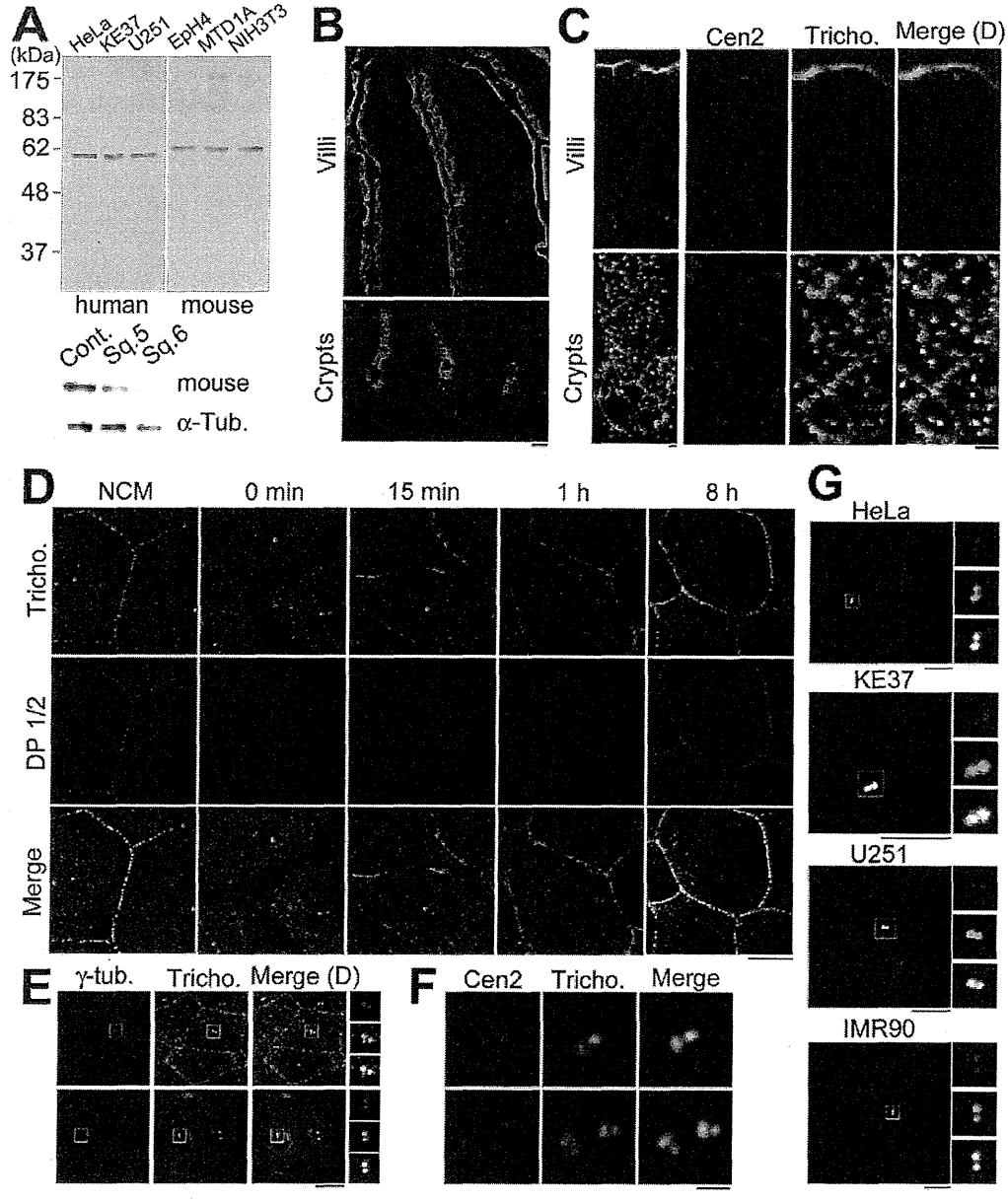

Fig. 1. Trichoplein is localized at the centrosome in proliferating cells. (**A**) Characterization of an anti-human or mouse trichoplein antibody by immunoblotting of indicated cell lysates. In lower panels, EpH4 cells were treated with control (Cont.) or mouse trichoplein-specific siRNA (Sq.5 or Sq.6) for 48 hours. (**B**,**C**) Localization of trichoplein (Tricho.; green) and centrin-2 (Cen2; red) in mouse small intestine. Nuclei were also stained with DAPI (D; blue) in these and subsequent panels. (**D**) Ca^{2+}-switch experiments. MTD1A cells were incubated in low-Ca^{2+} medium (DMEM with 0.05 mM $CaCl_2$) for 17–18 hours and then switched to normal growth medium containing >1.8 mM Ca^{2+} to induce cell junction assembly. Treated cells were subjected to immunocytochemistry with anti-mouse trichoplein and anti-desmoplakin (DP1/2) at the indicated time after switching. NCM indicates cells incubated in normal Ca^{2+} medium containing 10% FBS without the switch. (**E**–**G**) Trichoplein localization in EpH4 (E,F), HeLa, KE37, U251, or IMR90 (G) cells. Red indicates staining with anti-γ-tubulin (E) or anti-centrin-2 (F,G). Boxes in main image indicate centrosome structures shown at high magnification (E,G). Scale bars: 10 μm (B,D,E), 1 μm (C,F), 5 μm (G).

small interfering RNAs (siRNAs) reduced immunoreactivity to this band (Fig. 1A), confirming the specificity of this antibody. We next stained mouse small intestine with the anti-mouse trichoplein antibody. In absorptive epithelial cells, the antibody signals were primarily observed at the cell–cell border where desmoplakin was localized (supplementary material Fig. S1A,B). Especially in the villi, where cells are well differentiated, the signals were also detected as bundles at the apical region (Fig. 1B,C). These staining patterns confirm the previous observation that trichoplein localizes to keratin IFs and desmosomes in the epithelia (Nishizawa et al., 2005).

To elucidate the behavior of trichoplein during the formation of cell–cell attachment, we performed a Ca^{2+}-switch experiment (Fig. 1D). In MTD1A cells, trichoplein was concentrated at the cell–cell contact during cultivation in normal Ca^{2+} medium (NCM); localization of trichoplein almost completely overlapped with desmoplakin in the cell–cell contact area. In low-Ca^{2+} medium, where cell junctions do not form, trichoplein almost disappeared from the cell periphery (Fig. 1D, '0 minutes'). Within 15 minutes of increasing the Ca^{2+} concentration, trichoplein formed a linear structure at the cell–cell contact area. Because it took longer to concentrate desmoplakin in the cell–cell contact area after Ca^{2+} switching (Fig. 1D; also see supplementary material Fig. S1C), trichoplein appeared to have translocated to the cell–cell contact area before desmosome formation. Trichoplein colocalized at the desmosome with desmoplakin at 8 hours after the switch (Fig. 1D).

In addition to keratin IFs and desmosome, trichoplein appeared to localize to anti-centrin-2-positive punctate structures (which implies that they are centrioles) (Paoletti et al., 1996; Laoukili et al., 2000) in the crypt where dividing cells exist (Fig. 1B,C). Such a phenomenon was less observed in the villi where cells cannot divide (Fig. 1B,C). In EpH4 mouse mammary epithelial cells, anti-mouse trichoplein signals overlapped with anti-γ-tubulin-positive spots (which implied centrosomes), although they were also prominent at the cell-cell contact in cells with higher confluency (Fig. 1E). As shown in Fig. 1F, the number of anti-mouse trichoplein signals at the centrosome exactly coincided with the number of anti-centrin 2-positive spots (corresponding to the centriole number). The signals of anti-human trichoplein (Nishizawa et al., 2005) (also characterized in Fig. 1A) overlapped with anti-centrin 2-positive spots in human cultured cells, such as HeLa (cervical carcinoma), KE37 (T-cell leukemia), U251 (glioma) and IMR90 (fibroblast) cells (Fig. 1G). In HeLa cells, which express keratins, the antibody signals were also observed on keratin IFs (supplementary material Fig. S1D), as reported previously

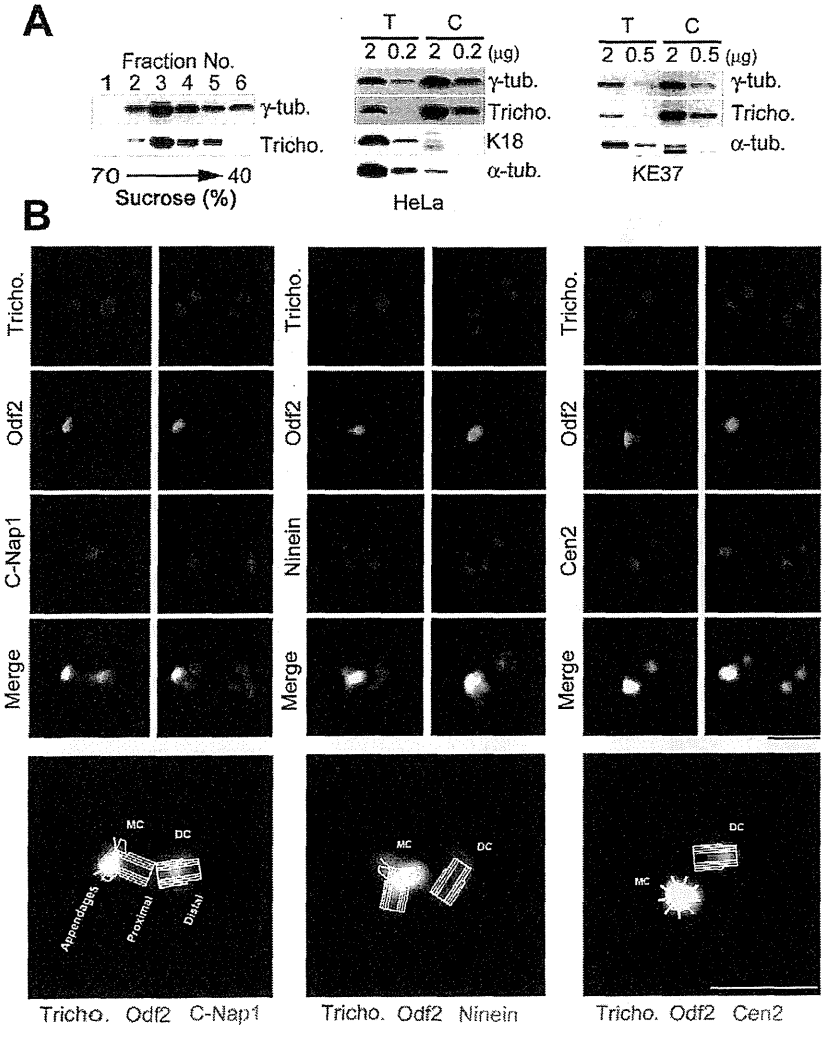

Fig. 2. Trichoplein localizes at the subdistal to medial zone of centrioles. (**A**) Western analyses of centrosomal fractions derived from HeLa (left or middle) or KE37 (right) cells. Each fraction (left), centrosome-enriched fraction (C) or total cell lysate (T; middle or right) was subjected to immunoblotting with the indicated antibodies. The amount of applied protein (μg) is also indicated on the top of each lane (middle or right). (**B**) Comparison of the localization between trichoplein and indicated centriolar marker proteins. Bottom micrographs are shown with cartoons, which indicate the structure of a mother or daughter centriole (MC or DC). Scale bars: 1 μm.

(Nishizawa et al., 2005). To confirm the existence of trichoplein in the centrosome, we prepared centrosomal fractions from HeLa or KE37 cells (Moudjou and Bornens, 1998). As shown in Fig. 2A, trichoplein was enriched in the centrosomal fractions, where γ-tubulin, but not keratin-18 or α-tubulin was concentrated (Fig. 2A). All these observations suggest that trichoplein is ubiquitous in both mother and daughter centrioles at a proliferative phase of the cell cycle.

To examine more precisely the localization of trichoplein on the centriole, HeLa cells were stained with several centriolar markers, together with anti-human trichoplein (Fig. 2B). One of the trichoplein signals partially overlapped signals of an antibody against Odf2 (outer dense fiber protein 2), a protein with distal to subdistal appendages on the mother centriole (Lange and Gull, 1995; Nakagawa et al., 2001; Ishikawa et al., 2005). However, the centriolar localization of trichoplein was different from that of C-Nap1 (centrosome-associated protein CEP250) (Fig. 2B, left panels), which localizes to the proximal ends of centrioles (Fry et al., 1998; Mayor et al., 2000). Anti-ninein signals were detected as four dots (Fig. 2B, middle panels), corroborating previous reports that ninein is localized not only at subdistal appendages of a mother centriole, but also at its proximal end (Mogensen et al., 2000; Ou et al., 2002; Delgehyr et al., 2005). Trichoplein signals were observed among three dots of anti-ninein signals (Fig. 2B, middle panels), which probably represent signals at subdistal appendages and the proximal end of a mother centriole (Fig. 2B, bottom micrographs with a cartoon). In addition, trichoplein partially overlapped with centrin-2 (Fig. 2B, right panels; also see Fig. 1F), a protein found at the distal ends of centrioles (Paoletti et al., 1996; Laoukili et al., 2000). All these results suggest that trichoplein is localizes to the subdistal to medial zone of a mother or daughter centriole.

This specific localization raised the question as to whether trichoplein interacts with ninein and Odf2. We first transfected COS7 cells with His-tagged trichoplein and GFP-tagged ninein and Odf2. His–trichoplein and each GFP-tagged protein were co-immunoprecipitated using an anti-GFP antibody (supplementary material Fig. S2A) and co-purified by Ni-NTA affinity chromatography (supplementary material Fig. S2B). Yeast two-hybrid analyses confirmed an interaction of trichoplein with ninein and Odf2 (supplementary material Fig. S3A), which was similar to that with keratin IF (Nishizawa et al., 2005). Immunoprecipitation analysis using an anti-human trichoplein antibody revealed that endogenous trichoplein formed a complex with endogenous ninein and Odf2 (Fig. 3A). GST pull-down assays using each purified protein indicated that trichoplein directly bound Odf2β (also called

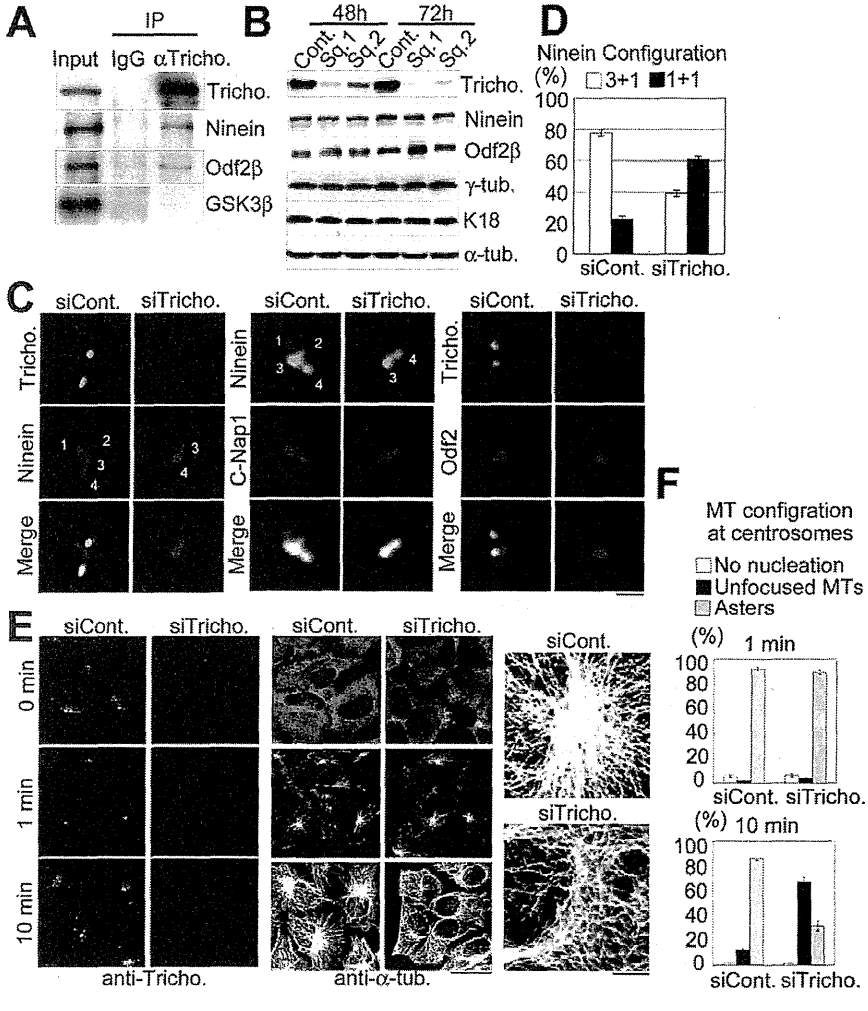

Fig. 3. Trichoplein controls ninein recruitment at appendages and microtubule anchoring at the centrosome.
(**A**) Immunoprecipitation (IP) assays using rabbit anti-human trichoplein. We used the same amount of rabbit IgG as a negative control (IgG). 2.5% of cell extract was also applied in the 'Input' lane. (**B**) HeLa cells treated with control (Cont.) or trichoplein-specific siRNA (Sq.1 or Sq.2) for 48 or 72 hours were subjected to immunoblotting with the indicated antibodies. (**C–F**) Effects of trichoplein depletion on localization of ninein or Odf2 (C,D) or MT regrowth assays after cold depolymerization (E,F). High magnification views on right indicate MT structures around the centrosome at 10 minutes after warming (E). Scale bars: 1 μm (10 μm for magnifications in E). Quantification data of ninein configuration (D) or MT morphology from centrosomes (F) in each group of cells are also indicated. The latter (F) were classified into the following three groups: no MT nucleation (white bars), unfocused MT network (black bars), and aster formation (gray bars). We analyzed 100 (D) or 400 (F) cells. Data are mean ± s.e.m. values from three independent experiments.

Cenexin) (Soung et al., 2006; Soung et al., 2009) and ninein in vitro (supplementary material Fig. S3B). These observations together suggest that trichoplein binds ninein and Odf2, probably through direct protein–protein interaction.

We next examined the effect of trichoplein depletion by RNA interference (RNAi). The treatment with human trichoplein-specific siRNAs induced the reduction of trichoplein protein level 48 or 72 hours after transfection (Fig. 3B). Because this treatment was unlikely to affect total protein levels of other centrosomal components such as ninein or Odf2β (Fig. 3B), we analyzed the change in their localization. As shown in Fig. 3C,D, in cells transfected with control siRNA, most anti-ninein signals were observed as three spots [which probably represent two separate signals (dots number 1 and 2) of subdistal appendages and one signal (dot number 3) of the proximal end on a mother centriole] plus one spot [which probably represents one signal (dot number 4)] at the proximal end on a daughter centriole (referred to as 3+1 patterns). However, in the trichoplein knockdown (KD) cells, anti-ninein signals diminished specifically at two spots. Because the remaining dots overlapped with C-Nap-1 (Fig. 3C), a proximal marker protein (Fry et al., 1998; Mayor et al., 2000), trichoplein depletion impaired ninein localization at the subdistal appendages of a mother centriole (dots number 1 and 2) but not at proximal ends of mother and daughter centrioles (dots number 3 and 4), which resulted in 1+1 patterns. However, the localization of Odf2 was not apparently affected by the reduction of trichoplein (Fig. 3C). These results suggest that trichoplein is required for ninein recruitment to subdistal appendages of a mother centriole but not to the proximal ends of both centrioles.

This requirement of trichoplein for ninein recruitment led us to perform MT-regrowth assays after cold depolymerization (Fig. 3E,F) (Luders et al., 2006; Yan et al., 2006), because ninein is reportedly required for MT anchoring (Dammermann and Merdes, 2002; Delgehyr et al., 2005). In cells transfected with both control siRNA and trichoplein-specific siRNA, a small centrosomal MT aster was visible 1 minute after warming. After 10 minutes, control cells had assembled an extensive array of cytoplasmic MTs that were centered at the centrosome. However, trichoplein depletion impaired this MT regrowth from the centrosome, although it did not affect the formation of cytoplasmic MTs. Trichoplein knockdown (KD) cells contained a cytoplasmic MT array that was similar in MT density to controls, but differed in that it did not have a radial, centrosome-based organization. These results suggest that trichoplein is required for MT anchoring at the centrosome.

To explore more precisely the relationships among trichoplein, ninein and Odf2, we transfected cells with ninein- (Fig. 4A,B) or Odf2-specific siRNAs (Fig. 4C,D). The reduction of ninein (Fig. 4A) or Odf2 (Fig. 4C) protein induced only marginal changes in total protein levels of the other components including trichoplein. Immunocytochemical analysis also revealed that ninein depletion induced only marginal changes in the centrosomal localization of trichoplein or Odf2 (Fig. 4B). However, Odf2 depletion abolished the recruitment of trichoplein to a mother centriole, although trichoplein localization at a daughter centriole appeared normal in Odf2 KD cells (Fig. 4D). As in trichoplein KD cells (Fig. 3C,D), anti-ninein signals diminished specifically at two spots in Odf2 KD cells (1+1 patterns; Fig. 4D,E). The rescue experiments confirmed that the observed abolition of trichoplein or ninein was attributed directly to specific depletion of trichoplein (Fig. 4F,G) or Odf2 (Fig. 4H-J), respectively. These observations suggest that Odf2 is required not only for the recruitment of trichoplein to a mother centriole, but also for ninein localization at subdistal appendages. Because the depletion of ninein or Odf2 (Fig. 4K-M) induced phenomena that were similar to those of trichoplein (Fig. 3E,F) in MT regrowth assays, we considered that Odf2, trichoplein and ninein cooperatively regulated MT anchoring at a mother centriole.

In the present study, we found that trichoplein, which was originally identified as a keratin IF scaffold protein (Nishizawa et al., 2005), is a component of centrioles at the subdistal to medial zone in proliferating cells. Ishikawa and co-workers (Ishikawa et al., 2005) reported that deletion of the Odf2 locus disrupted mother centriole appendages and eliminated two appendage-specific ninein dots, a phenomenon similar to that observed here in the case of RNAi-mediated Odf2 depletion (Fig. 4D). The present study thus indicates the way in which Odf2 controls ninein localization specifically at the subdistal appendages. Odf2 controls trichoplein localization specifically at a mother centriole (Fig. 4D) and then trichoplein recruits ninein specifically to subdistal appendages (Fig. 3C). Together with ninein (Mogensen et al., 2000; Delgehyr et al., 2005; Yan et al., 2006), trichoplein and Odf2 are indispensable to MT-anchoring activity at the centrosome (Fig. 3E,F and Fig. 4K-M). Because ninein depletion did not apparently affect the localization of two proteins (Fig. 4B), trichoplein and Odf2 might well regulate MT anchoring through the recruitment of ninein specifically to appendages. This notion is consistent with previous reports that ninein localizes to appendages and then makes a preferred docking site for MT attachment at the centrosome (Mogensen et al., 2000; Dammermann and Merdes, 2002; Ou et al., 2002; Delgehyr et al., 2005; Yan et al., 2006).

Odf2 is only required for trichoplein recruitment to the mother centriole: trichoplein localization to the presumptive daughter centriole appears normal when Odf2 is depleted (Fig. 4D). In addition, Odf2 (Fig. 4D) and trichoplein (Fig. 3C) are only indispensable for the localization of appendage-associated ninein. So, the interaction among these proteins might occur only around appendages (the subdistal end of a mother centriole) and thus be required for MT anchoring.

Since it binds Odf2 or ninein in a two-hybrid or purified protein system (supplementary material Fig. S3), trichoplein might directly engage Odf2 and appendage-associated ninein in vivo. However, this model appears to conflict with immunocytochemical observations that trichoplein does not completely overlap with Odf2 or ninein in a mother centriole (Fig. 2B). There are four possibilities to explain this: (1) the complex between trichoplein and Odf2 or ninein forms (probably in the cytoplasm) only before recruiting these proteins to a mother centriole; after the recruitment, these molecules are separated and then localized to distinct compartments; (2) other protein(s) might mediate the complex formation between trichoplein and Odf2 or ninein; (3) only a minor population of trichoplein directly binds Odf2 or ninein at a mother centriole, which is functionally more than enough; (4) trichoplein acts as a template for formation of the subdistal appendage. Regardless of these ideas, trichoplein works as a key mediator between Odf2 and appendage-associated ninein.

Odf2β and ninein reportedly regulate different cellular events (Ishikawa et al., 2005; Soung et al., 2006; Lechler and Fuchs, 2007; Moss et al., 2007; Soung et al., 2009). Odf2β depletion reduced the cell population at G1–S phase and elevated the population at S or G2–M phase (Soung et al., 2006). Because trichoplein depletion showed a similar FACS profile in HeLa cells (supplementary material Fig. S4), normal cell cycle progression

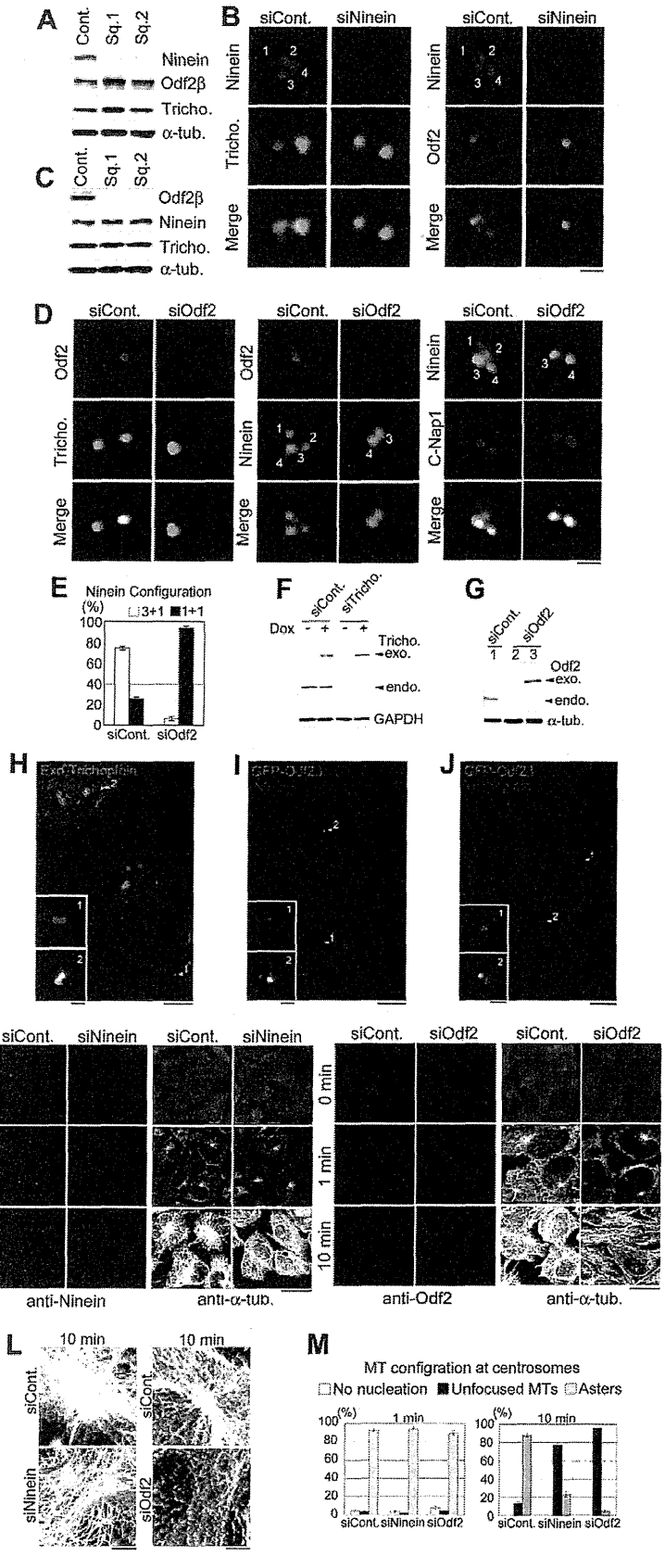

Fig. 4. Odf2 control recruitment of trichoplein and ninein at the distal end of a mother centriole. (**A–E**) Effects of depletion of ninein or Odf2 on other components. HeLa cells were treated with siRNAs specific to ninein (A,B) or Odf2 (C–E) for 96 hours. Then, cells were subjected to immunoblotting (A,C) or immunofluorescence (B,D) with the indicated antibodies. Scale bars: 1 μm. Quantification data of ninein configuration in each group of cells is indicated in E. (**F,H**) Rescue experiments of trichoplein siRNA in HeLa cells where MBP-trichoplein–FLAG is expressed in a tetracycline/doxycycline-dependent manner (Tet-ON HeLa cells). Cells were transfected with a negative control siRNA (siCont.) or trichoplein Sq.2 siRNA (targeting the 3′ UTR: siTricho.). Four hours after transfection, we removed the transfection medium and added a new growing medium with (+) or without (–; F) 100 ng/ml doxycycline. 48 hours after transfection, cells were subjected to immunoblotting with anti-trichoplein (to detect both endogenous and exogenous trichoplein) or anti-GAPDH (F) or immunofluorescence with anti-MBP (to detect only exogenous MBP-trichoplein–FLAG) and anti-ninein (H). (**G,I**) Rescue experiments using human-specific Odf2 siRNA2 and mouse GFP–Odf2β transfection. We transfected HeLa cells with the mixture of control (siCont.) or Odf2-specific (siOdf2) siRNA, pEGFP vector carrying mock (lanes 1, 2) or Odf2β (lane 3 in G), and Lipofectamine™ 2000 reagent. 48 hours after transfection, cells were subjected to immunoblotting with anti-Odf2 (to detect both endogenous and exogenous Odf2) or anti-α-tubulin (G) or immunofluorescence with anti-GFP (to detect only exogenous GFP–Odf2β) and anti-ninein (I) or anti-trichoplein (J). Scale bars: 1 μm (insets), 10 μm (H-J). (**K–M**) Effects of depletion of each protein on MT regrowth assays after cold depolymerization. Experiments were performed as described in Fig. 3E,F.

might require functional interaction between trichoplein and Odf2. However, ninein depletion had little impact on the cell cycle profile (Mikule et al., 2007), and the recruitment of ninein to appendages by Odf2 was dispensable for cell cycle regulation (Soung et al., 2009). Thus, trichoplein might regulate cell cycle progression independently of appendage-associated ninein. As for cell–cell contact, trichoplein (Fig. 1B,C and supplementary material Fig. S1A,B) (Nishizawa et al., 2005) and ninein (Lechler and Fuchs, 2007) are concentrated at the desmosome, although Odf2 does not appear to move to the cell–cell contact area (supplementary material Fig. S1C). Ninein is reported to move to desmosomes via desmoplakin and regulate MT dynamics during epidermal differentiation (Lechler and Fuchs, 2007). However, the Ca^{2+}-switch experiment revealed that trichoplein did not completely overlap with desmoplakin in the process of initial cell–cell contact formation: trichoplein appeared to be concentrated at the cell–cell contact area earlier than desmoplakin was (Fig. 1D). These observations overall suggest the possibility that trichoplein and ninein might have different roles in the formation of cell–cell contacts, at least before desmosome organization. Further studies to pursue the above possibilities and pinpoint the underlying mechanisms will be undertaken in future.

The present study documents the functional importance of a keratin IF scaffold protein trichoplein in MT anchoring at the centrosome and paves the way for future studies evaluating the inverse relationship between cell cycle progression and cell differentiation.

Materials and Methods

Preparation of recombinant proteins

His-tagged mouse trichoplein, MBP-human trichoplein or GST–ninein were expressed in BL21 CodonPlus® RP (Stratagene, La Jolla, CA) transformed with pET28a (Merck, Whitehouse Station, NJ) carrying mouse trichoplein, pMAL (New England Biolabs) carrying human trichoplein or pGEX (GE Healthcare, Milwaukee, WI) carrying ninein, respectively. We generated the recombinant baculovirus encoding GST–Odf2β using a combination of the GATEWAY™ vector conversion system and the Bac-to-Bac baculovirus expression system (Invitrogen). GST–Odf2β protein was expressed in the baculovirus-infected Sf9 cells. For production of an antibody against mouse trichoplein, His-tagged mouse trichoplein was purified on nickel-nitrilotriacetic acid-agarose resin (Qiagen; Valencia, CA) under 8 M urea denaturing conditions according to the manufacturer's protocol. For GST pull-down assay, each GST-fusion protein or MBP–trichoplein was purified under native condition through affinity chromatography with glutathione Sepharose™ 4B (GE Healthcare) or amylose resin (New England Biolabs) according to the manufacturer's protocol.

Antibodies

Anti-human and anti-mouse trichoplein antibodies were produced as described previously (Nishizawa et al., 2005). Antibodies from commercial sources were as follows: anti-centrin-2 (N-17), anti-GFP (B-2; Santa Cruz Biotechnology, Santa Cruz, CA); anti-pan-keratin, anti-keratin-18 (CY-90), anti-α-tubulin (B-5-1-2), anti-γ-tubulin (GTU-88) or anti-Odf2 (HPA001874; Sigma); anti-C-Nap1 (clone 42; BD Transduction Laboratories, San Diego, CA); anti-ninein (Poly6028; Biolegend, San Diego, CA); anti-desmoplakin-1 (DP-1), anti-desmoplakin-1/2 (clone DP1&2-2.15; DP1-2.17; DP1&2-2.20; Progen); anti-p38MAPK (#9212; Cell Signaling Technology); anti-MBP (ab9385; New England Biolabs); HRP-conjugated anti-GAPDH or anti-α-tubulin (ab15246; Abcam, Cambridge, UK); Anti-His (8916-1) or Anti-GFP (A. v. peptide; BD Clontech); and Anti-GFP (7.1 and 13.1; Roche, Basel, Switzerland). Western analyses were performed as described previously (Sugimoto et al., 2008).

Preparation of centrosomes

Centrosomes were isolated from KE37 and HeLa cells by discontinuous gradient ultracentrifugation according to the method of Moudjou and Bornens (Moudjou and Bornens, 1998). In brief, cells in the exponential phase of growth were treated with 1 μg/ml cytochalasin D and 0.2 μM nocodazole for 1 hour. Cells were collected by trypsinization and centrifugation and the resulting pellet was washed in TBS followed by 0.1× TBS with 8% sucrose. Cells were resuspended in 2 ml 0.1× TBS in 8% sucrose followed by addition of 8 ml lysis buffer (1 mM HEPES, pH 7.2, 0.5% NP-40, 0.5 mM $MgCl_2$, 0.1% β-mercaptoethanol, 1 μg/ml leupeptin, 1 μg/ml pepstatin, 1 μg/ml aprotinin and 1 mM PMSF). The suspension was gently shaken and passed five times through a 10 ml narrow-mouth serological pipette to lyse the cells. The lysate was spun at 2500 *g* for 10 minutes to remove swollen nuclei, chromatin aggregates and unlysed cells. The resulting supernatant was filtered through a nylon membrane followed by addition of HEPES buffer and DNaseI to a final concentration of 10 mM and 1 μg/ml, respectively, and incubated on ice for 30 minutes. The mixture was gently underlaid with 1 ml of 60% sucrose solution (10 mM PIPES pH 7.2, 0.1% Triton X-100 and 0.1% β-mercaptoethanol containing 60% w/w sucrose) and centrifuged at 10,000 *g* for 30 minutes to sediment centrosomes onto the cushion. The upper 8 ml of the supernatant was removed and the remainder, including the cushion containing the concentrated centrosomes, was gently vortexed and loaded onto a discontinuous sucrose gradient consisting of 70, 50, and 40% solutions from the bottom, respectively and centrifuged at 120,000 *g* for 1 hour. Fractions were collected and stored at –70°C before further analysis.

siRNA transfection

The following 21-nucleotide double-strand RNAs and negative controls (Negative Control and AllStars Neg. Control siRNA) were purchased from Qiagen: human trichoplein target sequence 1 (Sq.1), 5′-(AA)GAGCAGAGGAAACTGATTG-3′; human trichoplein Sq.2, 5′-(CA)GGGCATTGTTCCATGGTTA-3′; human trichoplein Sq.3, 5′-(CA)GTGTTTGGCCAGACATTAA-3′; human trichoplein Sq.4, 5′-(AA)GGCAGAATGGAGCTCTAAA-3′; mouse trichoplein Sq.5, 5′-(AA)GCTCTATCTCAGTATCAAA-3′; mouse trichoplein Sq.6, 5′-(CA)GGAATGCTTTATAAGTACA-3′; human ninein Sq.1, 5′-(CT)GGAAGAATATCGTGCACAA-3′; human ninein Sq.2, 5′-(AA)CGGGAACAAGAGAAGTTTA-3′. Human Odf2 siRNAs were purchased from Ambion (Austin, TX): Odf2 Sq.1, 5′-(CA)GGTCACTGTAAAATGAACC-3′ (11642); Odf2 Sq.2, 5′-(GA)GGTCAAGATGCAAAAAGGT-3′ (11735). We transfected cells with each siRNA using Lipofectamine™ RNAiMAX or Lipofectamine™ 2000 reagent, according to the manufacturer's protocol (Invitrogen). In some experiments, we repeated transfection(s) once or twice to increase the efficiency of reduction of each protein. Each set of experiments was performed under the same conditions including the siRNA concentration, frequency or interval of transfection and transfection reagent used. We obtained at least similar results using two target sequences of each protein (data not shown).

Plasmid transfection

We transfected cells with each set of vector(s) using Lipofectamine™ with Plus regent and Lipofectamine™ 2000 (Invitrogen) according to the manufacturer's instructions. We used pEGFP (BD Clontech) or pcDNA3 (Promega, Madison, WI) vector for the expression of EGFP-tagged or His-tagged protein, respectively.

Immunofluorescence microscopy and signal quantification

Cultured cells were grown on a coverslip coated with or without type I collagen (IWAKI Glass, Tokyo, Japan). KE37 suspension cells were attached on slide glasses (FRONTIER; Matsunami Glass, Osaka, Japan) before fixation. The fixation and immunostaining were performed as described previously (Sugimoto et al., 2008). Fluorescence image stacks (Fig. 3C, Fig. 4B,D and H–J) were obtained at 0.1–0.2 μm intervals in Z-section with an Olympus IX71 microscope equipped with a cooled charge-coupled device camera (CoolSNAP HQ; Roper Scientific, Princeton, NJ) and an UPlan SApo 100×/1.4 NA oil-immersion lens (Olympus, Tokyo, Japan) under the control of Metamorph software (Molecular Devices, Downingtown, PA). Then, the stacks were deconvolved and integrated with AutoDeblur and AutoVisualize × ver.1.4.1 (Molecular Devices). Confocal images (Fig. 1, Fig. 3E, Fig. 4K,L and supplementary material Fig. S1) were obtained as previously described (Sugimoto et al., 2008). The fluorescence intensity was determined after subtraction of the background using Zeiss AIM confocal software (Carl Zeiss, Thornwood, NY). Fig. 2B images were obtained by Delta Vision as described (Ishikawa et al., 2005). Immunohistochemistry was performed as described previously (Nishizawa et al., 2005).

Immunoprecipitation

HeLa cells (~3 ×10^6 cells) were lysed in 1 ml of lysis buffer [25 mM Tris-HCl, pH 7.5, 100 mM NaCl, 1 mM EDTA, 1 mM EGTA, 2.5 mM sodium pyrophosphate, 1 mM β-glycerophosphate, 1 mM sodium vanadate, 0.5% NP-40, 0.5% Empigen BB and protease inhibitor cocktail (Nacalai Tasque, Kyoto, Japan)] at 4°C for 10 minutes. After centrifugation (17,000 *g*) for 20 minutes, the supernatant was incubated with rabbit polyclonal anti-human trichoplein or rabbit IgG (each 2 μg) at 4°C for 3 hours. After centrifugation (17,000 *g*) for 20 minutes, the supernatant was rotated with 5 μl Protein-G–Sepharose™ (GE Healthcare) at 4°C for 20 minutes. After washing with lysis buffer three times, each immunoprecipitate was subjected to immunoblotting. For the detection of trichoplein, we used horseradish-peroxidase-conjugated anti-rabbit IgG (light chain-specific; Jackson ImmunoResearch Laboratories, West Grove, PA) as a secondary antibody.

GST pull-down assay

GST, GST–ninein, or GST–Odf2β (10 μg) was pre-incubated with 10 μl glutathione–Sepharose™ 4B (GE Healthcare) in binding buffer [50 mM Tris-HCl, pH 7.5, 150 mM NaCl, 1% Triton X-100, 1 mM EDTA and protease inhibitor cocktail (Nacalai Tasque)] for 1 hour at 4°C. After washing with binding buffer three times, the beads

were incubated with 10 μg MBP or MBP-trichoplein in 200 μl of the binding buffer for 1 hour at 4°C. After washing with the binding buffer three times, the beads were subjected to the immunoblotting with anti-MBP.

Establishment of Tet-ON HeLa cells

The rtTA-advanced segment and the tTS transcriptional silencer segment from pTet-On Advanced and pQC-tTS-IN (BD Clontech, Palo Alto, CA) were recombined into the retroviral vector pDEST-PQCXIP and pDEST-PQCXIN (Miyoshi et al., 1998), respectively, by the LR reaction (Invitrogen) to generate PQCXIN-Tet-On ADV and PQCXIP-tTS. The Elongation factor 1 alpha promoter (EF) in CSII-EF-MCS (a gift from Hiroyuki Miyoshi, RIKEN BioResource Center, Tsukuba, Japan) was replaced with a Tet-responsive promoter (TRE-Tight) from pTRE-Tight (BD Clontech) followed by a modified RfA fragment (Invitrogen) to make a Tet-responsive lentivirus vector, CSII-TRE-Tight-RfA. Fusion cDNAs with siRNA-resistant trichoplein were recombined into the lentiviral vector by the LR reaction (Invitrogen) to generate CSII-TRE-Tight-MBP-trichoplein-3xFLAG. Production and infection of recombinant retroviruses and lentiviruses were described as previously (Miyoshi et al., 1998; Sasaki et al., 2009).

We are grateful to Shoichiro Tsukita for providing EpH4 cells, Masatoshi Takeichi for MTD1A cells, Phillip James for pGBD-C1 and pGAD-C1 yeast two-hybrid vectors, Akira Kikuchi for providing mouse ninein cDNA and antibodies, Hiroyuki Miyoshi for CSII-EF-MCS and the related constructs, K. Kasahara for performing the immunoprecipitation in Fig. 3A, S. Yonemura and K. Kunimoto for helpful discussion, C. Yuhara and K. Kobori for technical assistance, Y. Takada for secretarial expertise, and M. Moore and J. Shields for critical comments on the manuscript. This work was supported in part by Grants-in-Aid for Scientific Research from the Japan Society for the Promotion of Science and from the Ministry of Education, Science, Technology, Sports and Culture of Japan; by a Grant-in-Aid for the Third Term Comprehensive 10-Year Strategy for Cancer Control from the Ministry of Health and Welfare, Japan; by the Uehara Memorial Foundation; by the Naito Foundation; by the Takeda Science Foundation; by a Research Grant from the Princess Takamatsu Cancer Research Fund; and by Astellas Foundation for Research on Metabolic Disorders.

Supplementary material available online at
http://jcs.biologists.org/cgi/content/full/124/6/857/DC1

References

Bettencourt-Dias, M. and Glover, D. M. (2007). Centrosome biogenesis and function: centrosomics brings new understanding. *Nat. Rev. Mol. Cell Biol.* **8**, 451-463.

Bornens, M. (2002). Centrosome composition and microtubule anchoring mechanisms. *Curr. Opin. Cell Biol.* **14**, 25-34.

Bornens, M. (2008). Organelle positioning and cell polarity. *Nat. Rev. Mol. Cell Biol.* **9**, 874-886.

Dammermann, A. and Merdes, A. (2002). Assembly of centrosomal proteins and microtubule organization depends on PCM-1. *J. Cell Biol.* **159**, 255-266.

Delgehyr, N., Sillibourne, J. and Bornens, M. (2005). Microtubule nucleation and anchoring at the centrosome are independent processes linked by ninein function. *J. Cell Sci.* **118**, 1565-1575.

Eriksson, J. E., Opal, P. and Goldman, R. D. (1992). Intermediate filament dynamics. *Curr. Opin. Cell Biol.* **4**, 99-104.

Eriksson, J. E., Dechat, T., Grin, B., Helfand, B., Mendez, M., Pallari, H. M. and Goldman, R. D. (2009). Introducing intermediate filaments: from discovery to disease. *J. Clin. Invest.* **119**, 1763-1771.

Fry, A. M., Mayor, T., Meraldi, P., Stierhof, Y. D., Tanaka, K. and Nigg, E. A. (1998). C-Nap1, a novel centrosomal coiled-coil protein and candidate substrate of the cell cycle-regulated protein kinase Nek2. *J. Cell Biol.* **141**, 1563-1574.

Fuchs, E. and Cleveland, D. W. (1998). A structural scaffolding of intermediate filaments in health and disease. *Science* **279**, 514-519.

Fuchs, E. and Weber, K. (1994). Intermediate filaments: structure, dynamics, function, and disease. *Annu. Rev. Biochem.* **63**, 345-382.

Godsel, L. M., Hobbs, R. P. and Green, K. J. (2008). Intermediate filament assembly: dynamics to disease. *Trends Cell Biol.* **18**, 28-37.

Houseweart, M. K. and Cleveland, D. W. (1998). Intermediate filaments and their associated proteins: multiple dynamic personalities. *Curr. Opin. Cell Biol.* **10**, 93-101.

Ishikawa, H., Kubo, A. and Tsukita, S. (2005). Odf2-deficient mother centrioles lack distal/subdistal appendages and the ability to generate primary cilia. *Nat. Cell Biol.* **7**, 517-524.

Izawa, I. and Inagaki, M. (2006). Regulatory mechanisms and functions of intermediate filaments: a study using site- and phosphorylation state-specific antibodies. *Cancer Sci.* **97**, 167-174.

Lange, B. M. and Gull, K. (1995). A molecular marker for centriole maturation in the mammalian cell cycle. *J. Cell Biol.* **130**, 919-927.

Laoukili, J., Perret, E., Middendorp, S., Houcine, O., Guennou, C., Marano, F., Bornens, M. and Tournier, F. (2000). Differential expression and cellular distribution of centrin isoforms during human ciliated cell differentiation in vitro. *J. Cell Sci.* **113**, 1355-1364.

Lechler, T. and Fuchs, E. (2007). Desmoplakin: an unexpected regulator of microtubule organization in the epidermis. *J. Cell Biol.* **176**, 147-154.

Luders, J., Patel, U. K. and Stearns, T. (2006). GCP-WD is a gamma-tubulin targeting factor required for centrosomal and chromatin-mediated microtubule nucleation. *Nat. Cell Biol.* **8**, 137-147.

Magin, T. M., Vijayaraj, P. and Leube, R. E. (2007). Structural and regulatory functions of keratins. *Exp. Cell Res.* **313**, 2021-2032.

Mayor, T., Stierhof, Y. D., Tanaka, K., Fry, A. M. and Nigg, E. A. (2000). The centrosomal protein C-Nap1 is required for cell cycle-regulated centrosome cohesion. *J. Cell Biol.* **151**, 837-846.

Mikule, K., Delaval, B., Kaldis, P., Jurcyzk, A., Hergert, P. and Doxsey, S. (2007). Loss of centrosome integrity induces p38-p53-p21-dependent G1-S arrest. *Nat. Cell Biol.* **9**, 160-170.

Miyoshi, H., Blomer, U., Takahashi, M., Gage, F. H. and Verma, I. M. (1998). Development of a self-inactivating lentivirus vector. *J. Virol.* **72**, 8150-8157.

Mogensen, M. M., Malik, A., Piel, M., Bouckson-Castaing, V. and Bornens, M. (2000). Microtubule minus-end anchorage at centrosomal and non-centrosomal sites: the role of ninein. *J. Cell Sci.* **113**, 3013-3023.

Moss, D. K., Bellett, G., Carter, J. M., Liovic, M., Keynton, J., Prescott, A. R., Lane, E. B. and Mogensen, M. M. (2007). Ninein is released from the centrosome and moves bi-directionally along microtubules. *J. Cell Sci.* **120**, 3064-3074.

Moudjou, M. and Bornens, M. (1998). Method of centrosome isolation from cultured animal cells. In *Cell Biology: A Laboratory Handbook* (ed. J. E. Celis), 111 pp. Orlando, FL: Academic Press Inc.

Nakagawa, Y., Yamane, Y., Okanoue, T. and Tsukita, S. (2001). Outer dense fiber 2 is a widespread centrosome scaffold component preferentially associated with mother centrioles: its identification from isolated centrosomes. *Mol. Biol. Cell* **12**, 1687-1697.

Nigg, E. A. and Raff, J. W. (2009). Centrioles, centrosomes, and cilia in health and disease. *Cell* **139**, 663-678.

Nishizawa, M., Izawa, I., Inoko, A., Hayashi, Y., Nagata, K., Yokoyama, T., Usukura, J. and Inagaki, M. (2005). Identification of trichoplein, a novel keratin filament-binding protein. *J. Cell Sci.* **118**, 1081-1090.

Ou, Y. Y., Mack, G. J., Zhang, M. and Rattner, J. B. (2002). CEP110 and ninein are located in a specific domain of the centrosome associated with centrosome maturation. *J. Cell Sci.* **115**, 1825-1835.

Paoletti, A., Moudjou, M., Paintrand, M., Salisbury, J. L. and Bornens, M. (1996). Most of centrin in animal cells is not centrosome-associated and centrosomal centrin is confined to the distal lumen of centrioles. *J. Cell Sci.* **109**, 3089-3102.

Pekny, M. and Lane, E. B. (2007). Intermediate filaments and stress. *Exp. Cell Res.* **313**, 2244-2254.

Sasaki, R., Narisawa-Saito, M., Yugawa, T., Fujita, M., Tashiro, H., Katabuchi, H. and Kiyono, T. (2009). Oncogenic transformation of human ovarian surface epithelial cells with defined cellular oncogenes. *Carcinogenesis* **30**, 423-431.

Soung, N. K., Kang, Y. H., Kim, K., Kamijo, K., Yoon, H., Seong, Y. S., Kuo, Y. L., Miki, T., Kim, S. R., Kuriyama, R. et al. (2006). Requirement of hCenexin for proper mitotic functions of polo-like kinase 1 at the centrosomes. *Mol. Cell. Biol.* **26**, 8316-8335.

Soung, N. K., Park, J. E., Yu, L. R., Lee, K. H., Lee, J. M., Bang, J. K., Veenstra, T. D., Rhee, K. and Lee, K. S. (2009). Plk1-dependent and -independent roles of an ODF2 splice variant, hCenexin1, at the centrosome of somatic cells. *Dev. Cell* **16**, 539-550.

Steinert, P. M. (1993). Structure, function, and dynamics of keratin intermediate filaments. *J. Invest. Dermatol.* **100**, 729-734.

Sugimoto, M., Inoko, A., Shiromizu, T., Nakayama, M., Zou, P., Yonemura, S., Hayashi, Y., Izawa, I., Sasoh, M., Uji, Y. et al. (2008). The keratin-binding protein Albatross regulates polarization of epithelial cells. *J. Cell Biol.* **183**, 19-28.

Yan, X., Habedanck, R. and Nigg, E. A. (2006). A complex of two centrosomal proteins, CAP350 and FOP, cooperates with EB1 in microtubule anchoring. *Mol. Biol. Cell* **17**, 634-644.

Published OnlineFirst December 3, 2010; DOI:10.1158/1078-0432.CCR-10-1287

Clinical Cancer Research

Forkhead Transcription Factor FOXO1 is a Direct Target of Progestin to Inhibit Endometrial Epithelial Cell Growth

Satoru Kyo, Junko Sakaguchi, Tohru Kiyono, et al.

Clin Cancer Res 2011;17:525-537. Published OnlineFirst December 3, 2010.

Published OnlineFirst December 3, 2010; DOI:10.1158/1078-0432.CCR-10-1287

Clinical Cancer Research

Forkhead Transcription Factor FOXO1 is a Direct Target of Progestin to Inhibit Endometrial Epithelial Cell Growth

Satoru Kyo[1], Junko Sakaguchi[1], Tohru Kiyono[2], Yutaka Shimizu[3], Yoshiko Maida[1], Yasunari Mizumoto[1], Noriko Mori[1], Mitsuhiro Nakamura[1], Masahiro Takakura[1], Kiyohiko Miyake[2], Masaru Sakamoto[4], and Masaki Inoue[1]

Abstract

Purpose and experimental design: Despite the therapeutic utility of progestin in invasive and preinvasive endometrial neoplasias, the molecular mechanisms through which it exerts inhibitory effects on endometrial epithelial growth are largely unknown. The aim of the study was to clarify the molecular mechanisms of progestin action to endometrial epithelial cells using originally established *in vitro* and *in vivo* treatment models for immortalized and transformed endometrial epithelial cell lines that express progesterone receptor.

Results: In this model, progestin effectively inhibited the cell growth, inducing G0/G1 arrest rather than apoptosis without p21/WAF-1 induction. Using DNA microarray analysis, we identified 24 genes whose expression increased more than 10-fold on progestin treatment. Of these genes, we paid special attention to forkhead box transcription factor *FOXO1*, known as a key gene for endometrial decidualization. Progestin markedly induced *FOXO1* gene expression mainly in the nuclei *in vitro* and *in vivo*. This induction was not due to the canonical activation of FOXO1 via protein dephosphorylation but due to *FOXO1* promoter activation and mRNA induction. siRNA inhibition of *FOXO1* significantly attenuated the effects of progestin to inhibit endometrial epithelial cell growth. Disrupting Akt activity by the introduction of the dominant negative form of *Akt* increased nuclear FOXO1 accumulation and enhanced the effect of progestin.

Conclusion: These findings suggest that *FOXO1* is a direct target of progestin, implicating novel molecular mechanisms of progestin to eradicate endometrial neoplasia. *Clin Cancer Res; 17(3); 525–37. ©2010 AACR.*

Introduction

Endometrial cancer accounts for approximately 50,000 annual deaths worldwide and is the most common invasive neoplasia of the female genital tract in North America, where the incidence is highest (22.0 per 100,000 people per year) (1). The prognosis of this type of cancer is relatively favorable, mainly because the disease is usually diagnosed while it is limited to the corpus of the uterus, in which case the lesions are surgically treated by hysterectomy and bilateral salphingo-oophorectomy with or without retroperitoneal lymphadenectomy. However, patients with disseminated disease or those who have recurrence at distant sites after initial surgery have few options for systemic therapy. Because low-grade endometrial cancer is susceptible to hormonal influences in a significant proportion of progesterone receptor (PR)-positive cases, progestin has been used as a treatment with recurrent or disseminated disease with such characteristics. Most studies have employed oral progestogens, including medroxyprogesterone acetate (MPA), which have response rates in the range of 11% to 56% (2).

Unlike invasive endometrial cancer, the prognosis of well-differentiated endometrial cancer without myometrial invasion is excellent, with a 5-year survival rate of more than 90% (3). Therefore, younger patients with these noninvasive diseases can opt for progestin therapy instead of surgery if they wish to preserve their potential for fertility. Superior response rates ranging from 70% to 90% have been reported for progestin therapy in patients with such early stages of endometrial cancer or preinvasive hyperplasia (4, 5).

Despite the therapeutic utility of progestin to invasive and preinvasive endometrial neoplasia, the molecular mechanisms of progestin's inhibitor effects on endometrial glands are largely unknown. Initial studies have demonstrated that

Authors' Affiliations: [1]Department of Obstetrics and Gynecology, Kanazawa University Graduate School of Medical Science, Kanazawa, Ishikawa, Japan; [2]Virology Division, National Cancer Center Research Institute, Chuohku, Tokyo, Japan; [3]Pharmaceutical Research Center, Mochida Pharmaceutical Co., Ltd., Gotemba, Shizuoka, Japan; and [4]Department of Gynecology, Kyoundo Hospital, Sasaki Institute, Tokyo, Japan

Note: Supplementary data for this article are available at Clinical Cancer Research Online (http://clincancerres.aacrjournals.org/).

Corresponding Author: Satoru Kyo, 13–1, Takaramachi, Kanazawa, Ishikawa 920–8641, Japan. Phone: 81-76-265-2425; Fax: 81-76-234-4266; E-mail: satoruky@med.kanazawa-u.ac.jp

doi: 10.1158/1078-0432.CCR-10-1287

Published OnlineFirst December 3, 2010; DOI:10.1158/1078-0432.CCR-10-1287

Translational Relevance

Endometrial cancer patients with recurrence at distant sites after initial surgery have few options for systemic therapy. Progestin [medroxyprogesterone acetate (MPA)] has been frequently used for such patients. Furthermore, younger patients with early stage endometrial cancer or endometrial hyperplasia can opt for progestin therapy instead of surgery if they wish to preserve their potential for fertility. However, efficacy of MPA varied among patients and no predictive parameter has been known, mainly due to lack of knowledge on the molecular mechanisms of progestin action to inhibit endometrial cell growth.

Our *in vitro* and *in vivo* treatment model has revealed that progestin directly induces FOXO via transcriptional activation to inhibit the growth of cancer and precancerous endometrial epithelial cells, indicating that FOXO is a novel target of MPA therapy, and Akt signaling, an upstream inhibitor of FOXO, is a potential predictor of MPA efficacy. This information will help define patient selection for progestin therapy.

progestin activates p21/WAF-1 expression, triggering cell cycle inhibition; therefore, p21/WAF-1 is a key effector of progestin action (6, 7). However, most studies have used breast cancer cell lines, whose response to progestin must be different from that of endometrial cells; for example, unlike endometrial cells, progestin occasionally has growth stimulatory effect on breast cancer cells *in vitro* and *in vivo*. Furthermore, either overexpression of ckd4 and/or cyclin D or dysfunction has been reported to frequently occur in a significant proportion of hormone-sensitive endometrial cancer, opposing p21/WAF-1 function (8–10), indicating that the p21/WAF-1 pathway is disrupted in endometrial carcinogenesis, and factors other than p21 may play crucial roles in exerting progestin action.

We have aimed to establish an *in vitro* and *in vivo* treatment model of progestin using immortalized and transformed endometrial epithelial cells expressing PR, and investigated the molecular mechanisms of progestin to inhibit the growth of endometrial glands. The microarray analyses identified the genes upregulated by progestin treatment, among which we noticed that the forkhead box O1 (*FOXO1*) gene plays a pivotal role in the progestin-mediated growth inhibition of the endometrial gland.

Experimental Procedures

Endometrial epithelial cell lineage and cell culture

EM-E6/E7/TERT cells are immortalized endometrial epithelial cells established by retroviral transduction of human papilomavirus (HPV) *E6/E7* genes together with human telomerase reverse transcriptase *(hTERT)* cDNA into primary endometrial epithelial cells purified from surgical specimens (11). EM-E6/E7/TERT/RAS cells are transformed cells with tumorigenicity in mice established by the additional introduction of oncogenic mutant *K-ras* alleles into EM-E6/E7/TERT cells (12). Although parental EM-E6/E7/TERT cells constitutively express weak levels of PR, EM-E6/E7/TERT or EM-E6/E7/TERT/RAS cells were further transfected with retroviral progesterone receptor B (PRB) expression vector (MSCVbsd-PRB) so that these transfectants, named EM-E6/E7/TERT/PR or EM-E6/E7/TERT/RAS/PR cells, strongly and stably expressed PRB (Fig. 1A). Akt signaling is one of the major inhibitory pathways for FOXO1 activity. To clarify the role of FOXO1 as a target of progestins, we introduced dominant negative alleles of *Akt* (*DN-Akt*) by retroviral transfer (12) into EM-E6/E7/TERT/PR cells to establish EM-E6/E7/TERT/PR/DN-AKT cells. These endometrial epithelial cell lines were basically maintained in Dulbecco's modied Eagle's medium (DMEM) supplemented with 10% fetal bovine serum (FBS) in an atmosphere of 5% CO_2 at 37°C. Tumorigenic endometrial epithelial cells were maintained in DMEM with 10% FBS. MCF-7 (Michigan Cancer Foundation-7) cells were purchased from the American Type Culture Collection and used as a positive control for progesterone receptor A (PRA) and PRB expressions. Ishikawa cells were kindly provided by Dr. Masato Nishida (National Kasumigaura Hospital, Tsuchiura, Japan).

RT-PCR assay

The expression of p21/WAF-1, PRB, and FOXO1 mRNAs was analyzed by reverse transcriptase-PCR (RT-PCR) amplification. The primer pairs used were: 5′-CCTCTTCGG-CCCAGTGGAC-3′ (forward),
5′–CCGTTTTCGACCCTGAGAG-3′ (reverse) for *p21/WAF-1*,
5′ – ACAGAATTCATGACTGAGCTGAAGGCAAAGGGT - 3′ (forward),
5′ – ACAAGATCTCAAACAGGCACCAAGAGCTGCTGA -3′ (reverse) for *PRB* (744–1173, 429 bp) (13),
5′–TGGACATGCTCAGCAGACATC-3′ (forward),
5′-TTGGGTCAGGCGGTTCA-3′ (reverse) for *FOXO1*.

For the detection of FOXO1 mRNA, EM-E6/E7/TERT or EM-E6/E7/TERT/PR cells were cultured in growth medium for 24 h and then incubated with or without MPA (10 nM) for different time periods. To examine whether FOXO1 mRNA expression depended on *de novo* protein synthesis, cycloheximide was simultaneously added with MPA at a final concentration of 10 μg/mL. Total RNA was then isolated from the cells using Isogen (Nippon Gene) according to the manufacturer's protocol, and cDNA was synthesized from 1 μg of RNA using the RNA PCR kit version 2 (TakaRa) with random primers. Typically, 2 μL aliquots of the reverse-transcribed cDNA were amplified by 28 cycles of PCR in 50 μL of 1× buffer [10 mM Tris-HCl (pH 8.3), 2.5 mM $MgCl_2$, and 50 mM KCl] containing 1 mM each of dATP, dCTP, dGTP, and dTTP, 2.5 units of Gene Taq (Nippon Gene), and 0.2 μM primers. Each cycle consisted of denaturation at 94°C for 30 s, annealing at 52°C for 30 s, and extension at 72°C for 45 s for p21/WAF-1 or FOXO1, or at 94°C for 1 min, annealing at 56°C for 1 min, and extension at 72°C for 1 min for PRB or PRAB. The PCR products were resolved by electrophoresis

Published OnlineFirst December 3, 2010; DOI:10.1158/1078-0432.CCR-10-1287

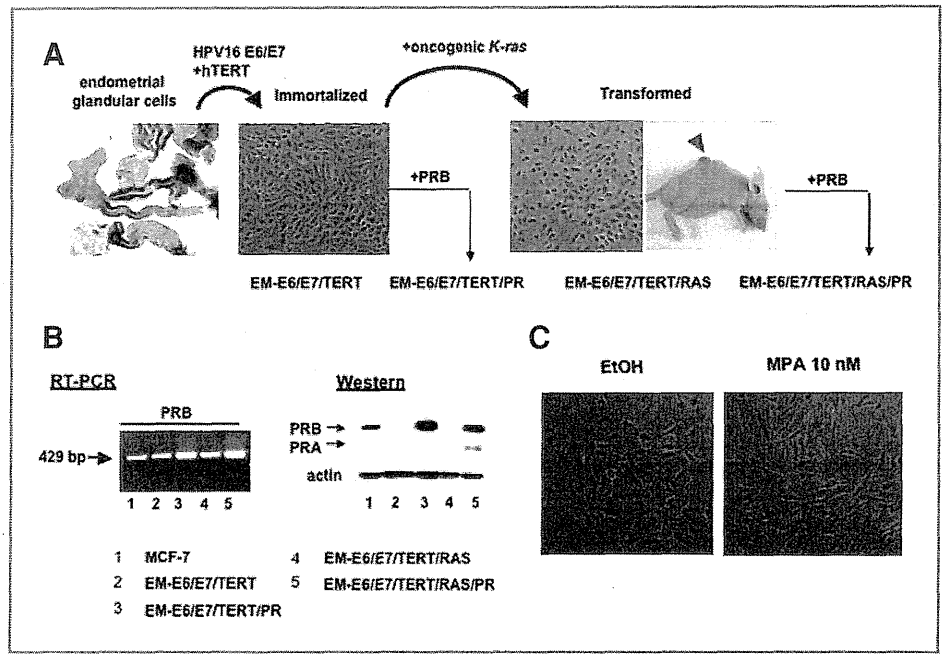

Figure 1. Endometrial epithelial cell lines used in the study. A, EM-E6/E7/TERT cells were immortalized cells generated from primary endometrial epithelial cells by the introduction of *HPV16 E6/E7* and *hTERT* genes (11). EM-E6/E7/TERT/RAS cells were generated from EM-E6/E7/TERT cells by the retroviral introduction of oncogenic mutant *K-ras* alleles, which produced transformed phenotypes, including anchorage-independent growth and tumorigenicity on nude mice (12). EM-E6/E7/TERT or EM-E6/E7/TERT/RAS cells were retrovirally transfected with *PRB* expression vector to achieve higher levels of PR expression. B, RT-PCR and western blot analyses were performed to confirm the expression of PR subtypes. PRA is an isoform of PR, lacking the N-terminal 164 amino acids of the larger isoform, PRB. The RT-PCR primers were designed to generate PRB products (429 bp) (15). The antibody against PR used in the western blot analysis recognized both PRA (81 kDa) and PRB (116 kDa), distinguishing each isoform by band size. MCF-7 cells were used as a positive control for PRA and PRB. C, change in cell shape of EM-E6/E7/TERT/PR cells following treatment with MPA for 72 h. Cells treated with MPA exhibited thinner and longer morphology.

on 7% polyacrylamide gels and stained with SYBR green I (FMC BioProducts). The efficiency of cDNA synthesis from each sample was estimated by PCR using glyceraldehyde 3 phosphate dehydrogenase (GAPDH)-specific primers as described previously (14).

Cell growth assay

Cells precultured in growth media for 24 h were incubated in 6-well plates in growth media or in serum-depleted media with phenol red-free DMEM in the absence or presence of MPA (MPA; 10 nM) or progesterone (10 nM), and cell growth was evaluated by counting the number of cells or measuring the incorporation of 5-Bromo-2′-deoxyuridine (BrdU) on the indicated days. The BrdU incorporation was detected using the DELFIA cell proliferation kit (PerkinElmer) according to the manufacturer's protocol as previously reported (15). EtOH was added so that its concentration was normalized to 0.1% in control and MPA- or progesterone-treated samples.

Cell cycle analysis

EM-E6/E7/TERT/PR cells were cultured in growth media in 6-well plates to 70%–80% confluence; then the media were replaced with serum-depleted phenol red-free DMEM and incubated for 24 h in the absence or presence of MPA at 10 nM. The cells were harvested and fixed overnight with 3 mL of ice-cold 80% ethanol. The fixed cells were then centrifuged, suspended in lysis buffer (100 mmol/L sodium citrate and 0.1% Triton X-100), and incubated for 15 min at room temperature before incubating with RNase A (10 mg/mL; Sigma Chemical) for 10 min at room temperature. DNA was stained with propidium iodide (50 μg/mL) for at least 1 h at 4°C. The DNA content was determined by flow cytometry (Beckman Coulter) and EXPO 32 software.

Western blot analysis

For examining PRA and PRB expressions, nuclear extracts were prepared from EM-E6/E7/TERT, EM-E6/E7/TERT/PR, EM-E6/E7/TERT/RAS, or EM-E6/E7/TERT/RAS/PR cells as previously described (16). For examining p21/WAF-1, PTEN, p-AKT, or FOXO1 expression, EM-E6/E7/TERT or EM-E6/E7/TERT/PR cells preincubated in growth media for 24 h were incubated in serum-depleted phenol red-free DMEM in the absence or presence of MPA or progesterone (10 or 100 nM) for various time periods; whole-cell extracts or nuclear or cytoplasmic extracts were prepared as previously described (16). Fifteen micrograms of the nuclear extracts or 50–100 μg of whole-cell or cytoplasmic extracts were electrophoresed on a SDS-polyacrylamide gel and transferred to polyvinylidine difluoride membranes.

Published OnlineFirst December 3, 2010; DOI:10.1158/1078-0432.CCR-10-1287

Membranes were blocked by immersion in TBST [150 mM NaCl, 20 mM Tris-Cl (pH 7.5), 0.1% Tween] containing 5% non-fat dried milk. They were then incubated with a specific antibody against PR [Progesterone Receptor Ab-8 (clone hPRa2+hPRa3); Lab Vision], p21/WAF (SC-469; Santa Cruz Biotechnology), PTEN [ABM-2052 (clone 6H2.1); Cascade BioScience], p-AKT (#4058; Cell Signaling Technology), or FOXO1 (#2880, Cell Signaling Technology). Next, the membranes were reacted with horseradish-peroxidase–conjugated anti-rabbit immunoglobulin (Jackson Immunoresearch Laboratories). The membranes were also probed with anti-actin antibody (Sigma) to normalize the differences among the samples. The LAS3000 CCD-Imaging System (Fujifilm Co. Ltd.) was used for detection and quantification of proteins visualized by Lumi-Light^{Plus} Western Blotting Substrate (Roche).

Nude mice xenograft experiments

EM-E6/E7/TERT/RAS or EM-E6/E7/TERT/RAS/PR cells were resuspended in a Hanks' balanced salt solution (Sigma) and subcutaneously injected (5×10^5 cells/mouse) at the base of the left flank of female 7- to 9-week-old ovariectomized BALB/c nu/nu mice (SLC). When tumors were seen after 3 weeks, hormone pellets consisting of placebo or progesterone (200 mg/pellet, 60-day release) (Innovative Research of America) were placed subcutaneously into the backs of the mice. Blood samples were collected from the tail vein, 10–14 days after pellet implantation, for measuring serum concentration of progesterone by ELISA (SRL, Inc.). Tumors were then monitored weekly for growth and were collected 4 weeks after pellet implantation. Half of the collected samples were stored for histological analysis after formalin fixation, while the other half were stored at −70°C until protein extraction.

Immunocytochemistry and immunohistochemistry

EM-E6/E7/TERT/PR cells were cultured on LAB TEK chamber slides (Nalge Nunc International) for 24 h and treated with or without MPA (10 nM) for 24 h. Then, the cells were fixed with 10% formaldehyde neutral buffer solution (37152-51; Nacalai Tesque, Inc.), immersed in methanol for 10 min at −20°C, blocked with PBS containing 10% goat serum and 0.3% Triton X-100 (166-11805; Wako Pure Chemical Industries, Ltd.) for 1 h at room temperature, and stained with monoclonal antibody to FOXO1 (#9462; Cell Signaling Technology) at 1:100 dilution for 12 h at 4°C. Next, they were incubated with fluorescent anti-rabbit IgG conjugates [Alexa Fluor 568 goat anti-rabbit IgG (H+L) highly cross-adsorbed, A11036; Invitrogen] for 1 h at room temperature in the dark. Cells were stained with 4′,6-diamidino-2-phenylindole (DAPI) (D1306; Invitrogen) for 3 min. Representative images were captured with a fluorescent microscope (Olympus BX-50; Olympus).

Immunohistochemical analysis was performed using formalin-fixed, paraffin-embedded specimens from mouse tumors formed with EM-E6/E7/TERT/RAS/PR cells. Sections were stained with a monoclonal antibody to FOXO1 (#9462; Cell Signaling Technology) at a 1:100 dilution for 12 h at 4°C. After the specimens were deparaffinized in xylene and graded alcohols, epitope retrieval was performed, in which the sections were heated in a microwave oven at 700 W for 10 min in 1 × Antigen Retrieval Solution (Biogenex). Then, endogenous peroxidase was blocked by immersing the sections in 0.3% H_2O_2 methanol for 30 min. The reaction was visualized with the EnVision Detection Kit (DAKO Cytomation) using diaminobenzidine tetrahydrochloride as the enzyme substrate. All sections were counterstained with GM hematoxylin stain solution (Muto Pure Chemicals Co., Ltd.). For negative controls, the non-reactive rabbit immunoglobulin fractions (X0903; Daco) or mouse IgG2a (X0943; Daco) was used, instead of the primary FOXO1 or cytokeratin antibodies, respectively.

DNA microarray analysis

For MPA-responsive gene expression profiling, EM-E6/E7/TERT/PR cells were cultured in growth medium for 24 h and then incubated with or without 10 nM MPA for 24 h.

The Agilent Whole Human Genome Oligo Microarrays (G4112A) containing 44,000 60-mer oligonucleotide probes representing 41,000 unique genes and transcripts were used for the experiments. Two types of total RNA samples were prepared: total RNA samples extracted from cells after 24 h with or without MPA treatment. Sample labeling and microarray processing was performed as detailed in the "One-Color Microarray-Based Gene Expression Analysis" (version 1.0, part number G4410-90040) protocol. Briefly, the Agilent One-Color Spike-Mix (part number 5188-5282) was diluted to 5,000-fold and 5 L of the diluted spike-in mix was added to 500 ng of each of the total RNA samples prior to labeling reactions. The spike-in mix consists of a mixture of 10 *in vitro* synthesized, polyadenylated transcripts derived from the adenovirus E1A gene. The labeling reactions were performed using the Agilent Low RNA Input Linear Amplification Kit (part number 5183-3523) in the presence of cyanine 3-CTP (Perkin Elmer part number NEL 580). For microarray hybridization, 500 ng of cyanine-3-labeled cRNA was fragmented and hybridized on the Agilent Whole Human Genome microarrays at 65°C for 17 h using the Agilent Gene Expression Hybridization Kit (part number 5188-5242). The hybridized microarrays were dissembled at room temperature in Gene Expression Wash Buffer 1 (part number 5188-5325), and then washed in the same buffer at room temperature for 1 min. This was followed by a 1-min wash in Gene Expression Wash Buffer 2 (part number 5188-5326) at an elevated temperature. The processed microarrays were scanned with the Agilent DNA microarray scanner (part number G2565BA) and extracted with Agilent Feature Extraction software (version 8.5, part number 2567AA). The resulting text files were loaded into the Agilent GeneSpring GX software (version 7.3) for further analysis.

The microarray data set was normalized in GeneSpring GX using the following scheme: First, data transformation:

Published OnlineFirst December 3, 2010; DOI:10.1158/1078-0432.CCR-10-1287

Intensity measurements less than 0.01 were set to 0.01. Second, per-chip normalization: Normalize to 70 percentile. Each intensity measurement on a microarray was divided by the 70-percentile intensity of all measurements on that microarray. Per-chip normalization removes any systemic error in signal intensities between chips. Third, per-gene normalization: Normalize to specific samples. For each gene, intensity values in all samples were normalized to the intensity value for that gene in the control samples. Per-gene normalization was carried out to investigate the relative gene expression of each sample after MPA treatment compared with specific control samples. We compared microarray data between samples with and without MPA treatment. Microarray data are supplied on our Supplemental Materials site.

Luciferase reporter assay

The 2.0 kb 5′-upstream region of the *FOXO1* gene (-1993 to -18: numbering based on the first ATG of *FOXO1* gene) was PCR-amplified from genomic DNA using primer set, 5′-CTAATTTTTCCTTTTTTCCCCTC-3′ (forward) and 5′-AGGGGCGGGGGTCACC-3′ (reverse), and inserted into the luciferase reporter plasmid pGL3-basic (Promega), named p-FOXO1-pro. EM-E6/E7/TERT/PR cells preincubated in growth media in 24-well dishes for 24 h were incubated in serum-depleted phenol red-free DMEM and transfected with 0.4 μg of reporter plasmid using Lipofectamin PLUS (Invitrogen Corp.) according to the manufacturer's protocol. Cells were simultaneously treated with 10 nM MPA for 48 h before being harvested and cell extracts prepared. Luciferase assays were performed using the Dual-Luciferase Reporter Assay System (Promega), in which Renilla luciferase plasmids were cotransfected as controls to standardize transcription efficiency. All experiments were performed at least three times for each plasmid, and the relative luciferase activity reported here is the mean of the three results.

siRNA inhibition assay

EM-E6/E7/TERT/PR cells were seeded overnight in the growth media in 6-well plates and transfected the next day with 25 nmol/L of non-specific scramble $siRNA_{control}$ (Ambion) or FOXO1A-specific siRNA (Ambion) using Lipofectamine 2000 reagent (Invitrogen) according to the manufacturer's recommendations. Forty-eight hours after transfection, cells were incubated in serum-depleted phenol red-free DMEM in the absence or presence of 10 nM MPA for 72 h before the cell number was counted in each sample to evaluate the effects of MPA on cell growth.

Statistical analysis

The data were basically presented as the mean ± SD of triplicated assays. Differences between groups were evaluated using Student's *t*-test. A *P* value of less than 0.05 was considered to indicate statistical significance.

Results

Progestin inhibits the growth of endometrial epithelial cell lines without p21/WAF-1 induction

We have previously established immortalized endometrial epithelial cells (EM-E6/E7/TERT cells) (Fig. 1A) (11) that sustain the functional characteristics of primary cells, including steroid responsiveness; estrogen treatment promoted cell growth *in vitro* whereas progestin treatment inhibited it, although these responsiveness weakened with increased population doublings. Tumorigenic endometrial epithelial cells (EM-E6/E7/TERT/RAS) were established by the additive introduction of oncogenic *mutant K-RAS* alleles into EM-E6/E7/TERT cells, which have the potential to form colonies on soft agar and tumors on nude mice (12). Basically, these immortal and transformed cells express weak levels of estrogen receptor α (ERα) as well as PR. To enhance the effect of progestin, stable cell lines expressing higher levels of PR were established by the additive introduction of *PRB* cDNA into immortal and transformed cells, named EM-E6/E7/TERT/PR and EM-E6/E7/TERT/RAS/PR cells, respectively. The expression of PR was then confirmed in these cells. RT-PCR assays confirmed that all these immortal cells expressed PRB. Western blot analysis revealed that EM-E6/E7/TERT/PR or EM-E6/E7/TERT/RAS/PR cells exhibited high levels of PRB expression with weak or faint levels of PRA expression (Fig. 1B), as shown in our recent study (15).

We first examined the effect of progestin on these cells *in vitro*. EM-E6/E7/TERT/PR or EM-E6/E7/TERT/RAS/PR cells were cultured in growth media and treated with 10 nM MPA for different time periods and the cell growth was monitored. The cells exhibited a longer and thinner morphology by the treatment with MPA (Fig. 1C). Significant growth retardation was observed after 4–5 days of treatment (Fig. 2A and B). In contrast, cells without PR overexpression (EM-E6/E7/TERT/vec or EM-E6/E7/TERT/RAS/vec) lacked the inhibitory effect of MPA (Fig. 2C and D), indicating that the growth inhibition was PR-dependent. We also confirmed MPA responsiveness in serum-depleted conditions as well (Supplementary Fig. 1). Significant growth inhibition was similarly observed in cells with PR overexpression but not those without it, although the extent of inhibition was lesser than cells incubated in growth media, probably because decreased proliferative activity by serum depletion masked the inhibitory effect of MPA. Furthermore, we tested the effect of another progestin, progesterone, on these cells. Progesterone inhibited the growth of EM-E6/E7/TERT/PR or EM-E6/E7/TERT/RAS/PR cells in a similar fashion (Fig. 2E and F) but not EM-E6/E7/TERT/vec or EM-E6/E7/TERT/RAS/vec cells (data not shown). Flow cytometric analysis revealed that MPA increased G0/G1 fractions by 5% to 6% and sub-G0/G1 fractions by 1% to 2% (Supplementary Fig. 2). To examine whether or not p21/WAF-1 was involved in MPA-induced growth retardation, we measured the change in p21/WAF-1 expression on treatment with MPA. RT-PCR assays or western blot analysis revealed that there was no

Published OnlineFirst December 3, 2010; DOI:10.1158/1078-0432.CCR-10-1287

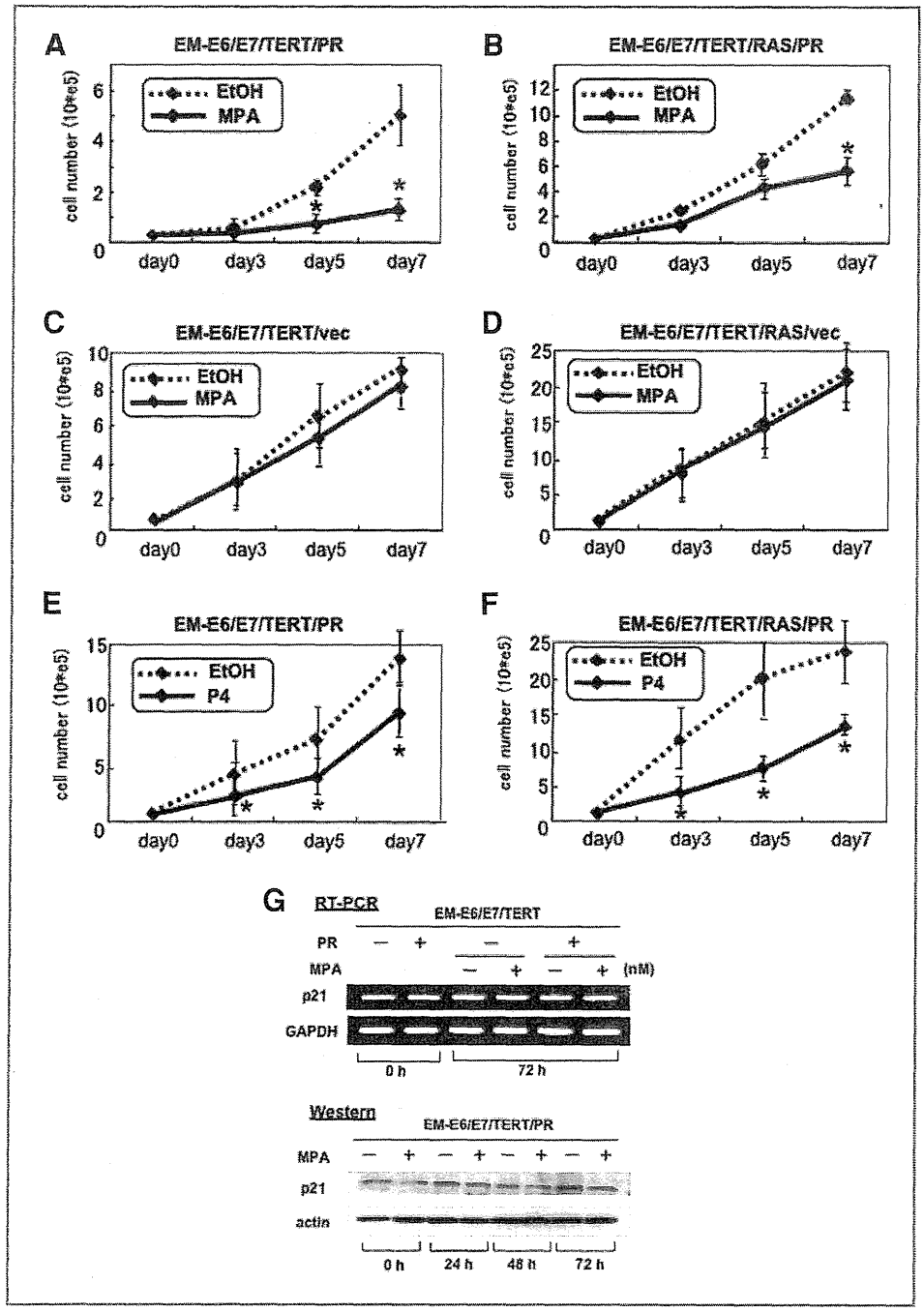

Figure 2. *In vitro* effect of progestin on the growth of endometrial epithelial cell lines. *In vitro* growth assay of endometrial epithelial cell lines treated with MPA or progesterone (P4). Cells were grown in growth media with or without 10 nM MPA (A–D) or progesterone (E and F) for different time periods; cell growth was determined by counting the cell number for each period. Note that MPA as well as progesterone significantly inhibited the growth of cells with PRB overexpression (A, B, E, and F) but not those without it (C and D). Each point represents the means ± SD of triplicate determinations in three independent experiments. *$P < 0.05$. G, analyses of the p21 expression upon MPA stimulation. EM-E6/E7/TERT or EM-E6/E7/TERT/PR cells were treated with or without MPA at 10 nM at different time periods, and RT-PCR and western blot analyses were performed.

significant induction of p21/WAF-1 mRNA or protein expression (Fig. 2G). Thus, p21/WAF-1 does not appear to play critical role in MPA-induced growth retardation.

We then examined the *in vivo* effects of progestin on the growth of tumorigenic endometrial cells. EM-E6/E7/TERT/RAS/PR cells were implanted to the flank of nude mice, and then progesterone pellets were inoculated after 3 weeks. Progesterone rather than MPA was selected because it is easy to measure its serum concentration using our available kit. As expected, progesterone concentration was significantly higher in treated groups than untreated groups [39.5 (15.1–73.2) vs. 7.5 (2.8–9.2) ng/mL, respectively]. As shown in Figure 3, tumors significantly decreased in size in treated groups. Taken together, these findings clearly show that progestin exerted an inhibitory effect on the cell growth of endometrial epithelial cell lineages both *in vitro* and *in vivo* in a p21/WAF-1–independent manner.

Published OnlineFirst December 3, 2010; DOI:10.1158/1078-0432.CCR-10-1287

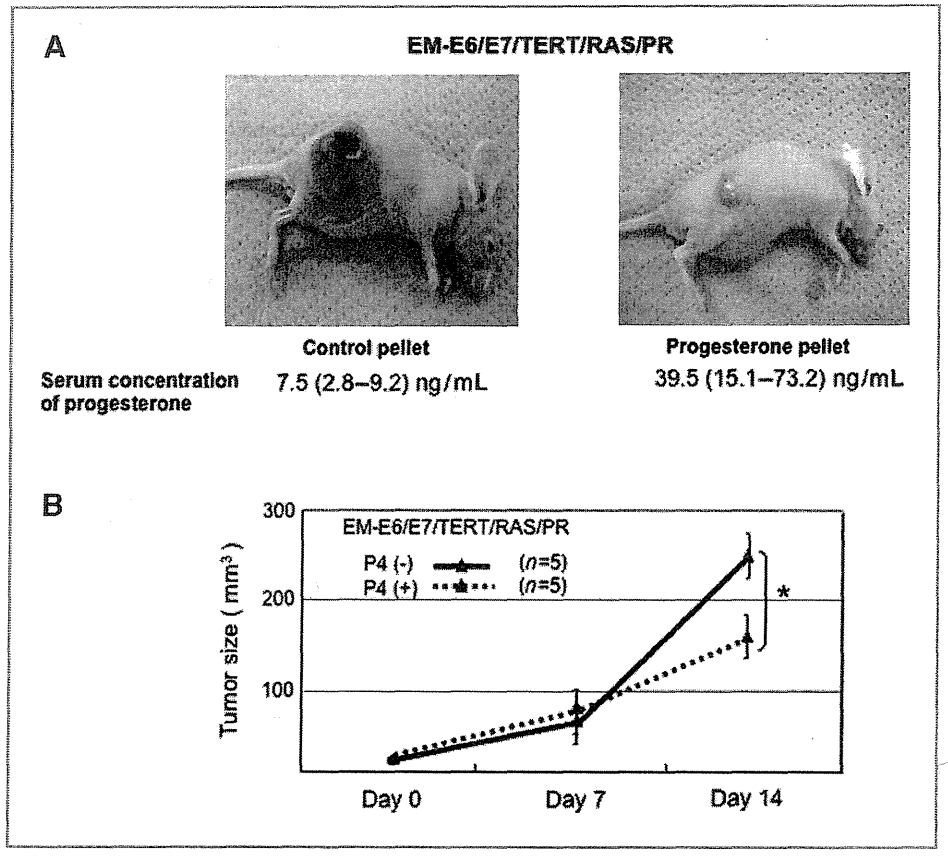

Figure 3. *In vivo* effect of MPA on the growth of endometrial epithelial cell lines. EM-E6/E7/TERT/RAS/PR cells were inoculated on the flank of mice. After tumor growth was confirmed, control placebo pellets or progesterone pellets were administrated subcutaneously, and then tumor growth was monitored. Mean serum concentration of progesterone was shown for each group. Data are presented as mean ± SD; $^*P < 0.05$.

Progestin induces FOXO1 expression via transcriptional activation in endometrial epithelial cell lines

To identify the molecular mechanisms of progestin's growth inhibitory effect on endometrial epithelial cell lines, we compared gene expression profiles of EM-E6/E7/TERT/PR cells treated and untreated with MPA. Of 44,000 transcripts included in the DNA microarray, we first defined the genes induced more than 10-fold by MPA stimulation and identified 24 of them (Supplementary Table 1). Of these genes, we noticed the *FOXO1* gene, because previous studies have found that progestin regulates the expression of *FOXO1* in endometrial stromal cells through subcellular translocation linked to its phosphorylation status, triggering endometrial decidualization and menstruation (17).

We therefore examined the change in expression and subcellular localization of FOXO1 in endometrial epithelial cell lines following treatment with progestin. EM-E6/E7/TERT or EM-E6/E7/TERT/PR cells were treated with MPA and western blot analyses performed using FOXO1-specific antibody. FOXO1 expression was significantly induced by treatment with MPA as well as progesterone at 10 or 100 nM in EM-E6/E7/TERT/PR cells (Fig. 4A) but not EM-E6/E7/TERT cells (data not shown). Induction was mainly observed in the nuclei, with only weak or faint levels of FOXO1 expression in the cytoplasm. Immunocytochemical analysis using EM-E6/E7/TERT/PR cells clearly showed that FOXO1 was mainly induced in the nuclei by MPA (Fig. 4B). Thus, progestin facilitates FOXO1 expression in a PR-dependent manner *in vitro*. This was not due to a change in the subcellular localization of FOXO1 (from cytoplasm to nucleus) because no significant FOXO1 expression was observed in the cytoplasm of untreated cells (Fig. 4A).

We then confirmed the induction of FOXO1 expression *in vivo* by the treatment with progesterone. Mouse tumors of EM-E6/E7/TERT/RAS/PR cells treated or untreated with progesterone pellets were collected and subjected to western blot analysis. As shown in Figure 4C, FOXO1 protein expression was upregulated by progesterone treatment in tumor tissues. Immunohistochemistry also showed that tumors exhibited marked induction of FOXO1 mainly in the nuclei when treated with progesterone (Fig. 4C).

We investigated the molecular mechanisms of FOXO1 induction upon MPA treatment. RT-PCR analysis was performed for FOXO1 mRNA expression using EM-E6/E7/TERT/PR cells treated or untreated with MPA. FOXO1 mRNA was significantly upregulated 8–72 h after the treatment (Fig. 5A). This activation was not blocked by treatment with cycloheximide, indicating that MPA directly activates FOXO1 mRNA expression without *de novo* protein

Published OnlineFirst December 3, 2010; DOI:10.1158/1078-0432.CCR-10-1287

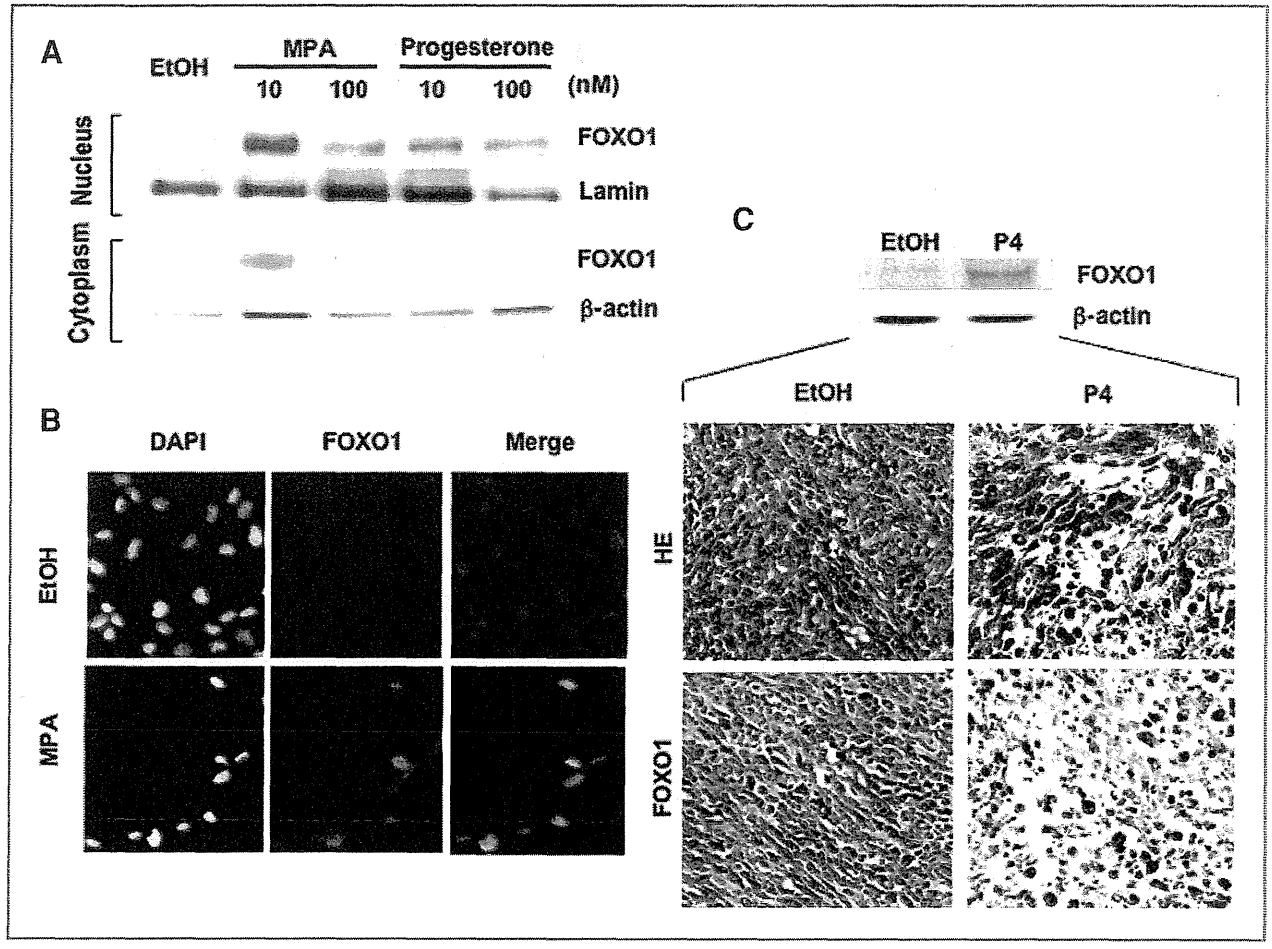

Figure 4. Induction of FOXO1 by progestin. A, EM-E6/E7/TERT/PR cells preincubated in growth media for 24 h were incubated in the serum-depleted phenol red–free DMEM in the absence or presence of MPA or progesterone for 48 h at the indicated concentrations. Nuclear or cytoplasmic extracts were collected from cells and the western blot analysis was performed using FOXO1 antibody. Lamin and β–actin were used as controls for nuclear or cytoplasmic protein loading, respectively. B, immunocytochemistry of FOXO1. EM-E6/E7/TERT/PR cells preincubated in growth media for 24 h were incubated on LAB TEK chamber slides for 24 h in the absence or presence of MPA for 24 h. After fixation, the cells were incubated with primary antibody to FOXO1, followed by fluorescent anti-IgG secondary antibody. The cells were also incubated with DAPI for nuclear staining and observed under a fluorescence microscope. Note that FOXO1 expression is induced preferentially in the nuclei (consistent with DAP staining) by MPA treatment. D, mouse tumors formed with EM-E6/E7/TERT/RAS/PR cells were treated with or without progesterone (P4) via subcutaneous injection of hormone pellets and were collected 4 weeks after the treatment. Then, whole-cell extracts were prepared, followed by western blot analysis for FOXO1. Immunohistochemistry of FOXO1 was also performed with matched samples of the EM-E6/E7/TERT/RAS/PR tumors treated with or without P4. HE staining of the tumor samples and induced FOXO1 expression mainly in the nuclei of the tumor cells are shown.

synthesis. We confirmed that this activation was not obvious in cells lacking PR-overexpression (EM-E6/E7/TERT cells) (Fig. 5A), suggesting that FOXO1 activation by MPA is PR-dependent. We further performed the luciferase reporter assays using *FOXO1* gene promoter spanning 2.0 kb sequences upstream of the first ATG. As shown in Figure 5B, MPA treatment of EM-E6/E7/TERT/PR cells activated the *FOXO1* promoter approximately by 3-fold, while no activation was observed in EM-E6/E7/TERT cells. These findings indicate that MPA directly induces FOXO1 expression via the transcriptional activation of *FOXO1*. To analyze the status of signaling pathway, which regulates subcellular localization of FOXO1, we examined the expression of PTEN and p-AKT as critical components of phosphatidylinositol 3-kinase (PI3K)/AKT pathway. As shown in Figure 5C, activation of PTEN expression or reduction of p-AKT expression, both of which facilitate nuclear retention of FOXO1, was not observed by the treatment with MPA.

FOXO1 mediates progestin to inhibit epithelial cell growth

To investigate the role of FOXO1 in the effect of progestin, a knockdown experiment for *FOXO1* was performed via siRNA inhibition. EM-E6/E7/TERT/PR cells were transfected with siRNA against *FOXO1* and treated

Published OnlineFirst December 3, 2010; DOI:10.1158/1078-0432.CCR-10-1287

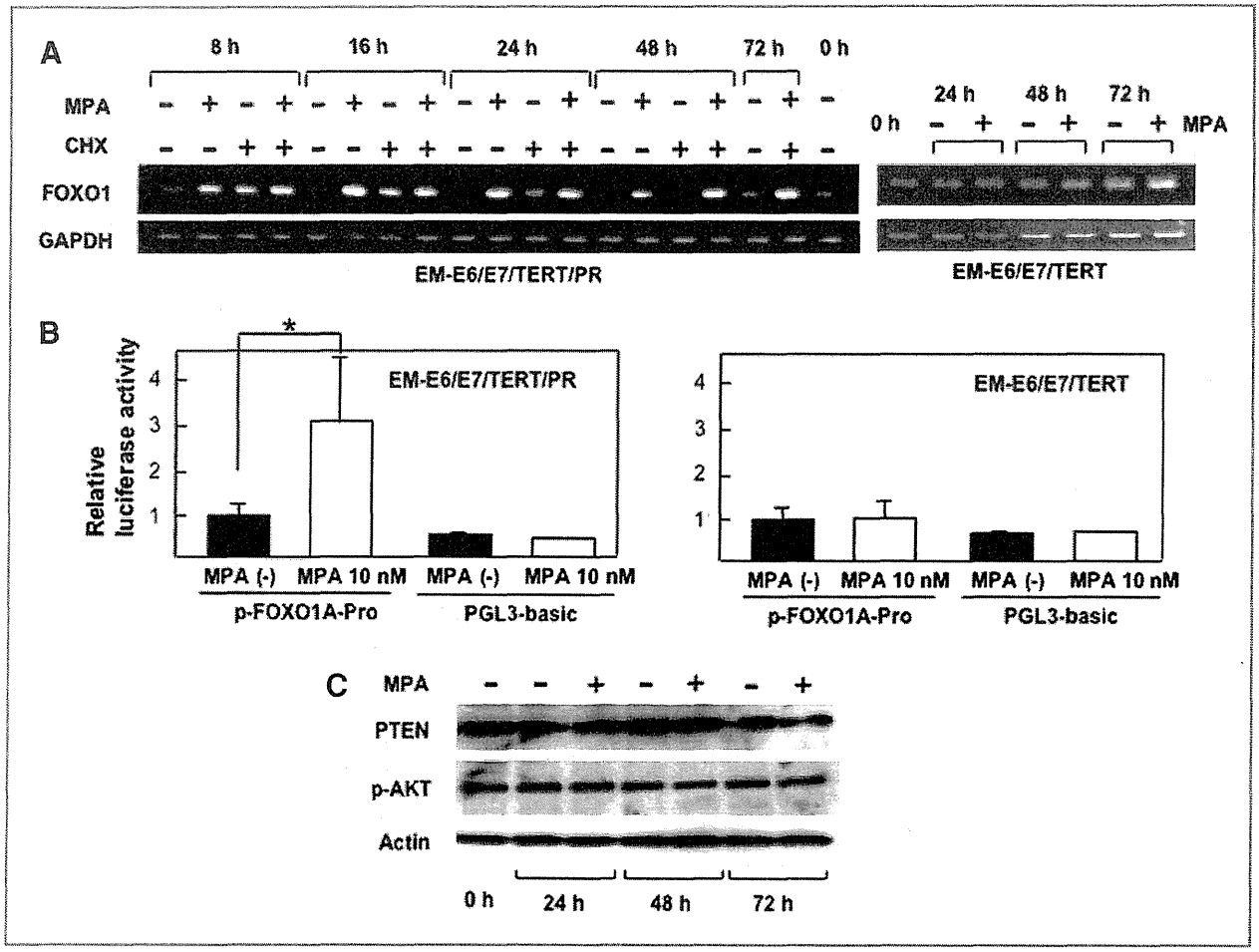

Figure 5. Mechanisms of FOXO induction by progestin. A, RT-PCR analysis of FOXO1 in EM-E6/E7/TERT/PR or EM-E6/E7/TERT cells. The cells were cultured with or without MPA in the presence or absence of cycloheximide (CHX) for different time periods and RNAs were collected and subjected to the RT-PCR for FOXO1. B, luciferase reporter assay using FOXO promoter. EM-E6/E7/TERT or EM-E6/E7/TERT/PR cells were transfected with luciferase reporter plasmid containing 2.0 kb of FOXO promoter or with blank reporter plasmid (pGL3-basic), followed by treatment with or without MPA. Seventy-two hours after treatment, cells were recovered and luciferase assays were performed. Relative luciferase activity is shown in each reporter plasmid. Data are presented as mean ± SD of the three independent experiments. *$P < 0.05$. C, EM-E6/E7/TERT/PR cells were treated with or without MPA at 10 nM and incubated at different time periods, followed by the western blot analysis for PTEN or p-AKT.

with or without MPA at 10 nM, followed by monitoring cell growth. Western blot analysis confirmed that knockdown was successful, exhibiting apparently decreased FOXO1 expression. These cells showed only minimally inducible FOXO1 expression on treatment with MPA (Fig. 6). In the absence of MPA, cells with knocked-down *FOXO1* had increased growth rate compared with those with control siRNA, indicating that endogenous FOXO1 plays some role in cell proliferation. Treatment with MPA significantly inhibited the growth of cells transfected with control siRNA, while the inhibition was largely abrogated in those with knocked-down *FOXO1*. Thus, the effect of MPA was attenuated via knockdown of *FOXO1*, supporting the role of FOXO1 in progestin action. We sought to confirm whether similar effect was observed in other endometrial cancer cell lines as well. *FOXO1* knockdown was performed in Ishikawa cells in the same way and MPA effect was examined (Supplementary Fig. 3). Ishikawa cells exhibited growth inhibition as well as FOXO1 induction by the treatment with MPA, but with lesser extent, probably due to very low levels of PR expression. FOXO1 knockdown effectively cancelled growth inhibition by MPA.

Akt signaling limits progestin action on endometrial epithelial cell growth

FOXO family members are direct downstream targets of the PI3K/Akt signal transduction pathway. Activation of PI3K/Akt signals phosphorylates FOXO proteins, resulting in cytoplasmic retention and inhibiting their transcriptional activity. Therefore, we speculated that Akt signaling might affect the action of progestin. To investigate this possibility, a special cell line, named EM-E7/E7/TERT/PR/DN-AKT, was established with an introduced dominant

Published OnlineFirst December 3, 2010; DOI:10.1158/1078-0432.CCR-10-1287

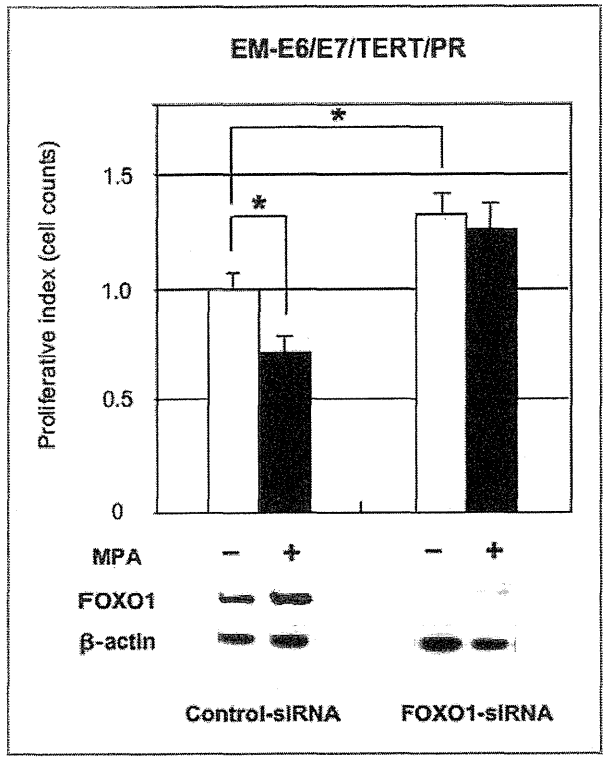

Figure 6. Role of FOXO1 in the action of progestin. EM-E6/E7/TERT/PR cells were transfected with non-specific scramble $siRNA_{control}$ or FOXO1-specific siRNA. Forty-eight hours after transfection, the cells were incubated with or without MPA at 10 nM for 72 h. Then, western blot analysis was performed to confirm the levels of FOXO1 expression. Simultaneously, cell number was counted in paired samples and shown as the relative value (proliferation index) in each sample to evaluate the effects of MPA. Data are presented as mean ± SD of the three independent experiments. $^*P < 0.05$.

negative allele of *Akt* gene from EM-E7/E7/TERT/PR cells. Introduction of the dominant negative allele of *Akt* gene has been confirmed to inhibit Akt function in endometrial epithelial cell lines (12). Both cells exhibited similar growth rate in the absence of MPA (Fig. 7A). We then compared the effects of MPA on these cells. Treatment with MPA at 10 nM led to 35% growth inhibition of EM-E7/E7/TERT/PR/vector cells on day 3 and 46% on day 6 (Fig. 7A). The same treatment in EM-E7/E7/TERT/PR/DN-AKT cells resulted in 56% growth inhibition on day 3 and 66% on day 6. Thus, introducing DN-AKT caused enhanced growth inhibition by MPA.

We next examined the extent of FOXO1 induction by MPA in the nuclei of both cells (Fig. 7B). The western blot analysis revealed the enhanced FOXO1 induction in EM-E7/E7/TERT/PR/DN-AKT compared with EM-E7/E7/TERT/PR/vector cells on days 3 and 6. Especially, most prominent induction of FOXO1 was observed in EM-E7/E7/TERT/PR/DN-AKT on day 6, when the maximal growth inhibition was confirmed in Figure 7A. These findings proved that Akt signaling is a critical factor that limits the progestin action to endometrial epithelial cells.

Discussion

FOXO1 is a member of the FOXO subfamily of the Forkhead/winged helix family of transcription factors that is involved in cell cycle regulation and apoptosis (17): the subfamily contains the mammalian members FOXO1 (Fkhr), FOXO3a (Fkhr-l1), and FOXO4 (Afx) (18, 19). The role of FOXO1 in endometrial biology has been known in relation to the process of decidualization (17, 20, 21). FOXO1 induces the expression of decidualization-specific genes of endometrial stromal cells, such as insulin-like growth factor binding protein 1 (*IGFBP1*), decorin (*DCN*), and prolactin (*PRL*): this is enhanced by the action of cyclic AMP (camp). Here, we focused on the roles of FOXO1 in progestin action on endometrial epithelial cells and clearly showed it to be a novel target of progestin to inhibit the growth of both non-tumorigenic and tumorigenic endometrial epithelial cells.

The canonical pathway of FOXO1 regulation has been thought to be on the PI3K pathway. Growth-factor–dependent activation of the PI3K pathway blocks the function of all FOXO members by Akt-dependent phosphorylation of their three conserved residues, which leads to inhibition of DNA binding, nuclear exclusion, and subsequent sequestration in the cytoplasm (22–24). Recently, a unique role of progestin in the survival of endometrial stromal cells has been reported by Labied and colleagues (17). According to their results, progestin treatment of stromal cells enhanced the expression of phosphorylated FOXO1, which, because it is strictly localized to the cytoplasm, is considered to be an inactive form. Withdrawal of progestin induced rapid nuclear translocation of FOXO1, which activated expression of *BIM*, a known FOXO target gene encoding for a proapoptotic Bcl-2 homology 3 domain-only protein (25). This unique role of FOXO1 in response to progestin withdrawal was demonstrated in differentiating stromal cells of the endometrium. On the other side, we found that progestin induced FOXO1 expression mainly in the nuclei upon progestin stimulation in endometrial epithelial cells. RT-PCR assay clearly showed that FOXO1 mRNA is upregulated approximately 4–8 h after treatment with MPA, even in the presence of cycloheximide. Luciferase reporter assays demonstrated that MPA upregulated the transcriptional activity of *FOXO* promoter. Therefore, our results support the direct transcriptional activation of *FOXO1* gene by progestin. Computer-assisted homology search found potential PR-binding sites that have a homology with the glucocorticoid receptor-responsive element on the *FOXO1* promoter (data not shown). We are currently confirming the specific interaction of PR with such sites on the *FOXO* promoter. What is the molecular mechanism of the nuclear FOXO1 accumulation upon progestin stimulation? The most probable scenario might be that MPA inhibits PI3K/AKT signaling pathway, leading to the nuclear FOXO1 translocation. However, we confirmed that PI3K/AKT pathway was not inhibited by MPA in endometrial epithelial cells (Fig. 5D). Alternatively, it is known that FOXO1 binds to PR in the nuclei (26) and this physical